STRUCTURAL ANALYSIS AND MICROSTRUCTURAL EXAMINATION OF THE CATOCTIN FORMATION IN THE SOUTH MOUNTAIN ANTICLINE, MARYLAND

By

ROBERT SPITZER

A thesis

Submitted to the School of Graduate Studies

in Partial Fulfilment of the Requirements

for the Degree

Bachelor of Science

McMaster University

April, 1979

BACHELOR OF SCIENCE (1979)
(Geology)

McMASTER UNIVERSITY
Hamilton, Ontatario.

TITLE: Structural Analysis and Microstructural Examination of the Catoctin Formation in the South Mountain Anticline, Maryland

AUTHOR: Robert Spitzer

SUPERVISOR: Professor P.M. Clifford

NUMBER OF PAGES: xii, 83

SCOPE AND CONTENTS:

The original shape of the deformed amygdules, as well the tectonic strain ellipsoid have been calculated mathemetically using several standard methods.

A deformation path has been constructed from measurements performed on the amygdules.

Investigation of microstructures found within amygdules and groundmass has been done.

Structural and microstructural analysis provide the basis of interpretation concerning the formation of features in the final fabric.

XZ SECTION

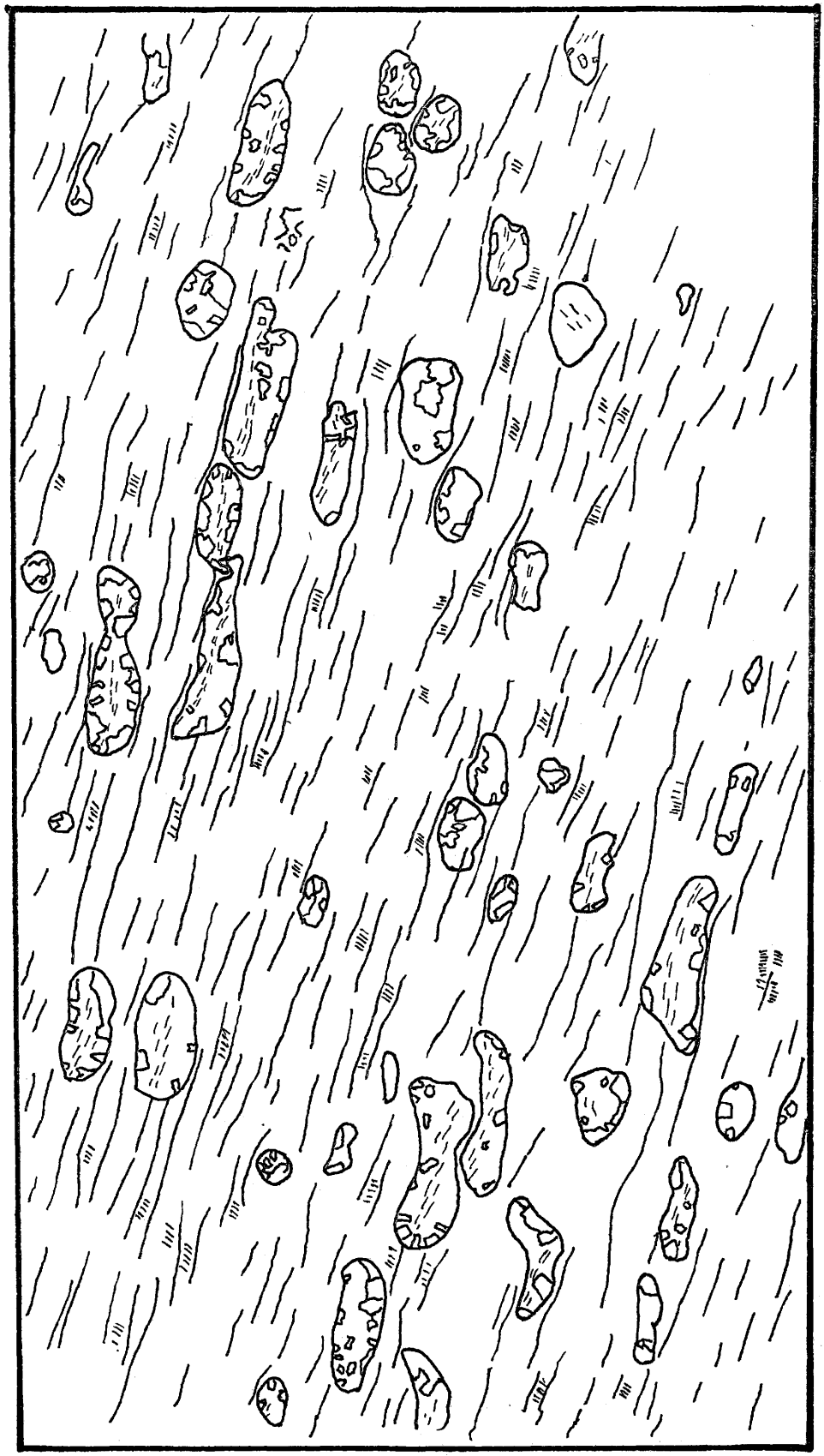

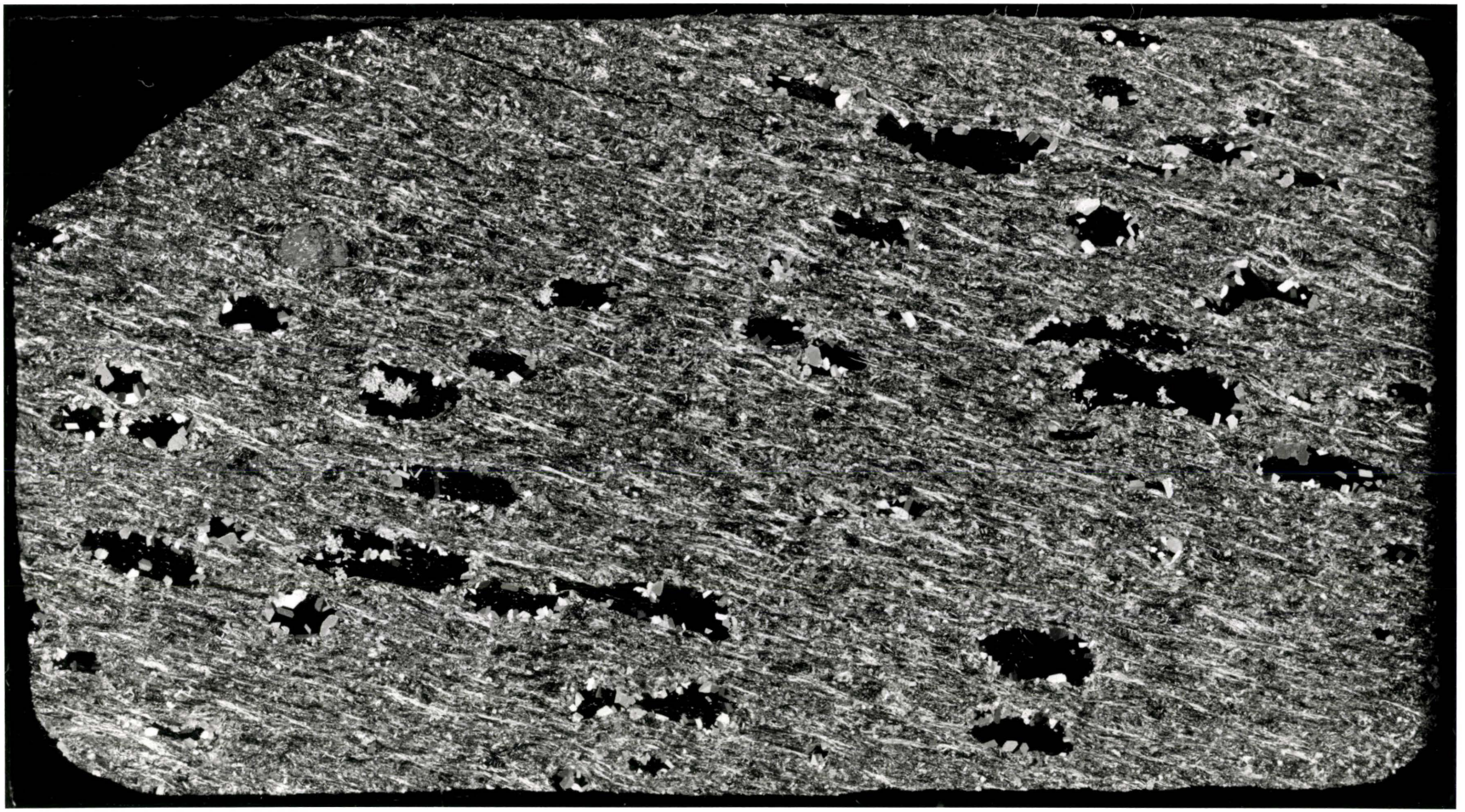

ACKNOWLEDGEMENTS

The writer would like to express his deep appreciation to Dr. Paul M. Clifford who suggested the thesis topic, contiually offered his time and assistance during the length of the project, and finally, examined the manuscript.

The writer also wishes to thank Dr. Burley and C. Gower in regard to discussion pertaining to the identification of various minerals.

Many thanks are also extended to John Whorwood for his photographic advice; to Len Zwicker for the thin section preparation; to Carol Hempstock for typewriting the final manuscript, and to all the others who have helped in any way.

TABLE OF CONTENTS

LIST OF FIGURES

LIST OF PLATES

ABSTRACT

Microstructural as well as structural analysis of amygdules and groundmass of the Catoctin Formation located in the overturned western limb of the South Mountain anticline permit interpretation pertaining to the nature of cleavage development. Various methods have been employed in the structural analysis of amygdules, in order to ascertain their original shapes and also the nature of the tectonic strain ellipsoid. A deformation path has been constructed in logarithmic co-ordinates. This appears to be an improvement over the arithmatic graph of Wood (1974). Microstructural investigation allows recognition of two distinct domains within the groundmass and amygdules ; i)an early schistosity and ii)a crenulation cleavage. Microstructural and structural analysis provide a logical explanation of this history. An initial flattening episode forming the early schistosity was followed by approximately plane strain deformation creating the crenulation cleavage.

CHAPTER I

INTRODUCTION

The area of study is located in the Catoctin Formation on the overturned limb of the South Mountain anticline in Maryland. Previous work in this area has been carried out by Cloos (1947) and Nickelsen (1956). Both authors describe a pervasive regional cleavage dipping eastward (fanning westward and upward) and extending from the Catoctin Formation through the overlying clastic sediments of the Chilhowee Group and into the Cambrian and Ordivician carbonates. Cloos (1947) and Nickelsen (1956) note that in the cleavage surfaces a consistent prominent lineation oriented normal to the fold axis exists. Although much of Cloos's work has been directed towards ooids found within the Chilhowee Group many of his findings are pertinent to features seen in the Catoctin Formation. Cloos maintains that the material has been transported in a westerly direction along these "regional" cleavage planes in "a sequence of events that began with an activation of the basement at depth and then a rise in westward creep with a push from "behind" and "within" the crystalline axis" (Cloos, 1971.p.xiv). The investigation of microstructures (within the Catoctin Formation) as well as structural analysis of amygdules may be useful in determination of the development of this "regional" cleavage as well as other features pertinent to the deformation.

The development of crenulation cleavage within volcanic rocks appears to be a rarity; due to the initial random fabric. An initial episode of flattening creating a weak schistosity , followed by a deformation appears to be responsible for the crenulation cleavage. The cleavage is not as well defined as those found in metasediments, however it is clearly present.

CHAPTER II

GEOLOGIC SETTING

1. GEOGRAPHIC LOCATION

The South Mountain structure is an elongate feature trending south south-east to north north-west from northern Virginia through Maryland and extending into southern Pennsylvania. The study area is situated on the northern side of U. S. 40, one and a half miles east of Cavetown, Maryland (Figure 1).

2. GEOLOGIC STRUCTURE

The major geologic structure in the South Mountain region is the South Mountain Anticline. The anticline has been mapped in several areas (Cloos, 1947, 1951; Whitaker, 1955; Nickelsen, 1956; Fauth, 1968). Cloos (1947) was the first to suggest the structure was a large anticline with smaller adjacent folds on the limbs. Detailed mapping on the eastern limb by Whitaker (1955) and the western limb by Nickelsen (1956) has confirmed Cloos's idea. The overturned monoclinal fold contains cleavage penetrating from the

FIG. 1 Location map illustrating the study area
(The western slope of the South Mountain Uplift)

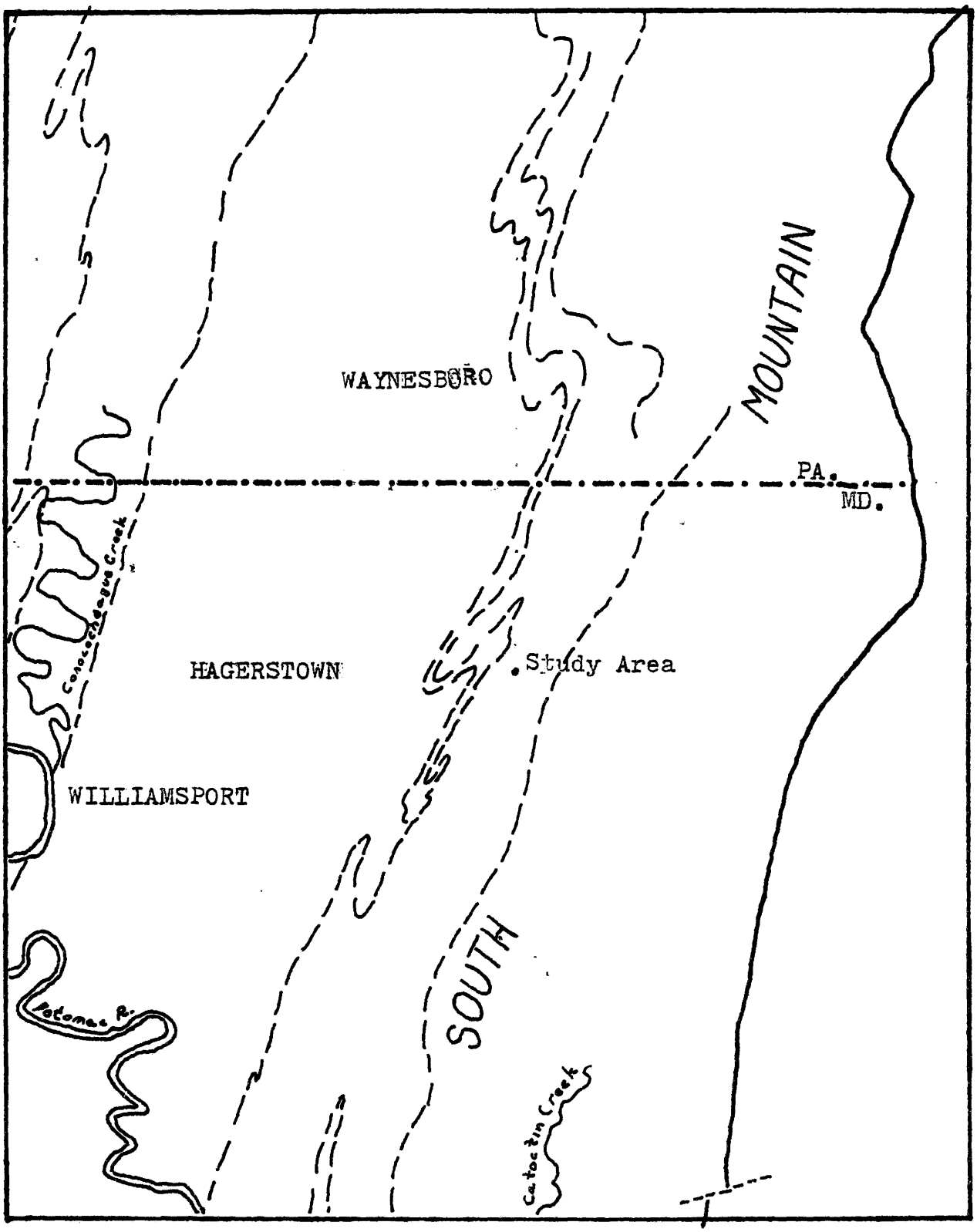

Catoctin Volcanics through the Chilhowee Formation and into the Great Valley carbonate sequence. The basement is presumably unfaulted except on the eastern limb where a much younger Triassic basin occurs. The geologic structure is presented in Figures 2 and 3. There is debate as to whether the structure is a large fold or a folded thrust sheet moved from the east. The fold hypothesis is preferable since there is no evidence of a detachment zone (essential if thrusting were involved) and due to the great size and transport distance involved (at least 50 km.) thrusting is unlikely. Formation of the structure probably occurred during the closing of the Atlantic in mid-Paleozoic time. The movement of material in the South Mountain structure appears to have been along cleavage planes upward and toward the west north-west.

3. STRATIGRAPHY

The stratigraphy is summarized in tabular form (Table 1). This study is on the Catocin Volcanics in the overturned western limb of the South Mountain Anticline.

FIG. 2 GEOLOGIC MAP of the northern part of the Blue Ridge showing the distribution of the Catoctin Formation and the location of South Mountain.

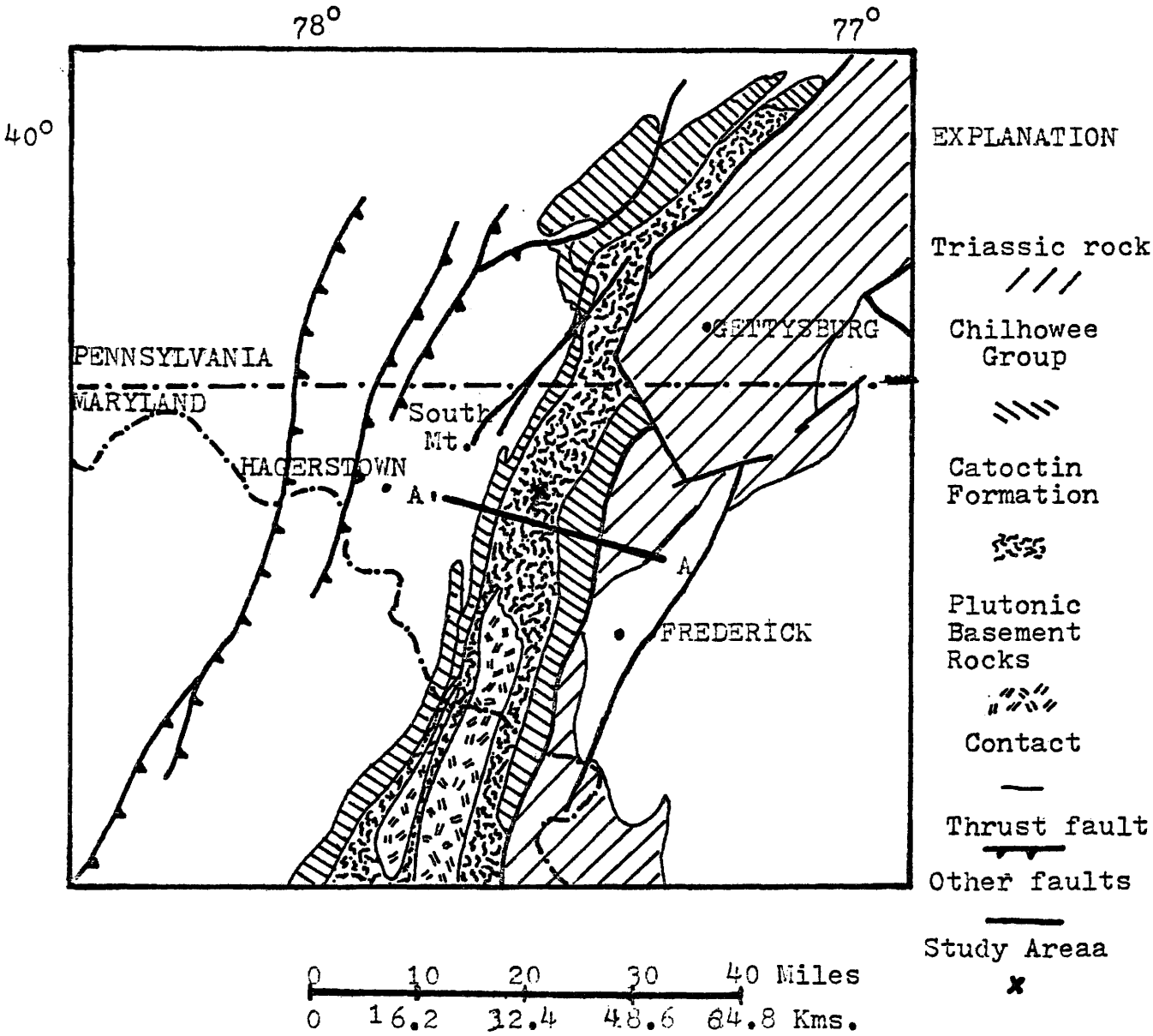

FIG.3. Structure section along A.A(of previous figure) north of Frederick, Md.(from Cloos 1947)

(Plate 13)

Explanation

- Rs - Triassic sandstone and shale
- Cl - Cambrian limestone,dolomite &shal
- Cc - Chilhowee Group (Cambrian)- quartzite and phyllite
- pCv - Catoctin and Swift Run Formations Upper Precambrian metabasalt, phyllite and quartzite
- pCg - Precambrian basement complex

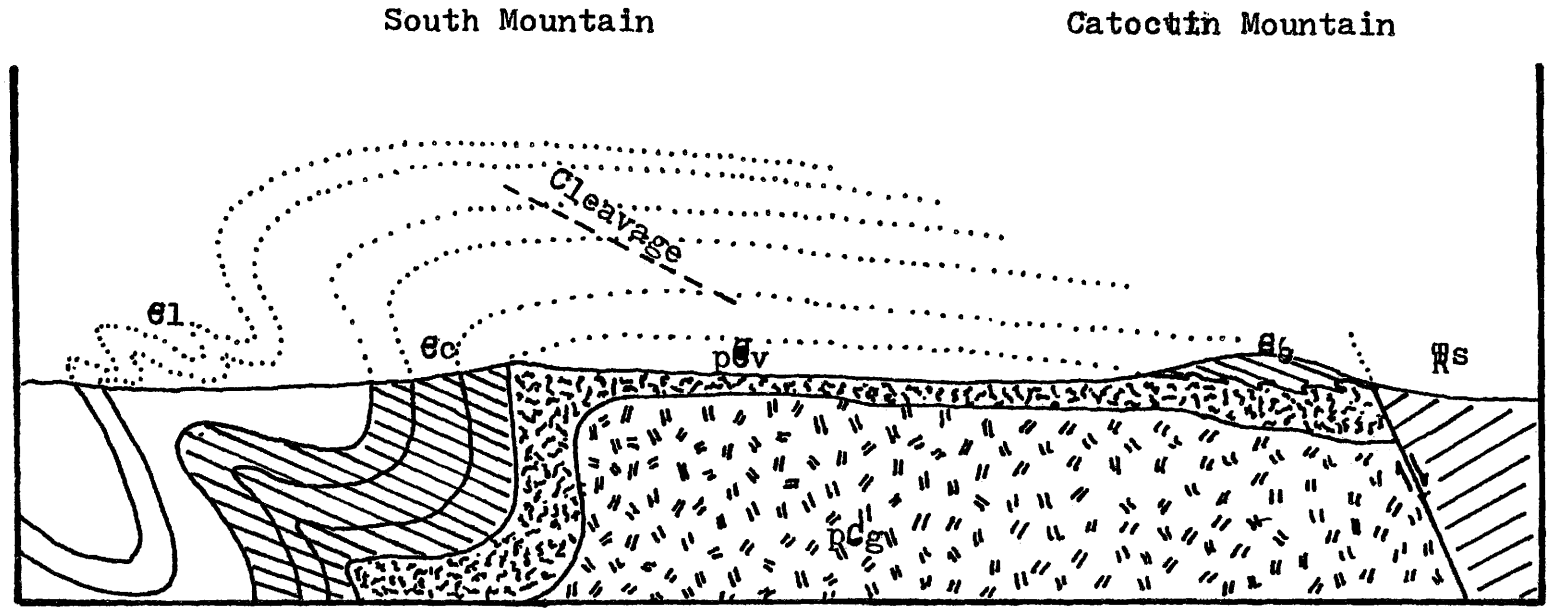

TABLE 1. THE PRE CAMBRIAN-CAMBRIAN STRATIGRAPHIC COLUMN

SYSTEM/GROUP	FORMATION	DESCRIPTION	THICKNESS (in feet)
	Harpers Formation	Gray phyllite and slate, banded with quartzite. Always with strong cleavage which tends to obliterate bedding. Repeated by folding. Thickened and altered in crest of South Mountain and Elk Ridge anticlines.	2000-2750
CAMBRIAN (LOWER) (Chilhowee Group)	Weverton Formation	Light gray to dark, purple-banded, granular to vitreous quartzite, partly cross-bedded with conglomerate layers. Thick-bedded white quartzite layers. Shaly beds between quartzites.	1250
	Loudon Formation	Highly ferruginous, dark, sandy phyllite and thin-bedded arkosic quartzite; conglomerate layers. Basal beds blue and green slate and conglomerate of unassorted pebbles of quartz and slate in slaty matrix.	150-450
		UNCONFORMITY	
PRE CAMBRIAN	Catoctin Formation	Metabasalt with amygdular layers and secondary quartz, calcite, and epidote. Closely folded and altered to hornblende-chlorite schist and greenstone. Metarhyolite: gray and purple slate and breccia.	100-400
		UNCONFORMITY	
		Gneissic hypersthene granodiorite, quartz monzonite, granite, syenite, anorthosite, and para-gneiss.	

4. CATOCTIN VOLCANICS

i) Macroscopic Features:

The Catoctin Volcanics are composed overwhelmingly of fine grained greenstone. The cleavage in the Catoctin Formation is the dominant structural macroscopic feature. According to Cloos (1947) the axial plane cleavage dips eastward (between 10^{o} and 50^{o}) and fans gradually to the west and upwards. The cleavage is a domainal feature. At certain localities (including the study area) cleavage is deflected around resistant masses within the rock, developing a "bulging cleavage" (Cloos, 1971; Reed, 1955). Macroscopically no cleavage is evident within the resistent rock. Extensive work by Cloos on ooids from the Chilhowee Group in the South Mountain area shows that the intensity of deformation is paralleled by the intensity of development of cleavage. Cloos proposes that ..."the anticlinorium is a large shear fold in which deformation took place by laminar flow along cleavage planes which caused such crustal shortening without important thrusting causing thickening at hinges and thinning at flanks." (Cloos, 1947, p. 901-902.).

Lineation is very common in greenstone, consisting of chlorite amygdules which are elongate and thin, parallel to cleavage planes and thin perpendicular to cleavage. In the massive resistant material (epidosite) lineation is not as

marked. Cloos (1947) states that the lineation ..."is probably (in the broadest sense) the direction of tectonic transport, slippage, growth, or extension and probably all of these." (Cloos, 1971, p. 56.). Zones of abundant amygdules have been interpreted as ancient flow tops. Cloos comments that ..."the chlorite blebs are elongated and well aligned,... they are excellent as direction markers but questionable as strain markers because one axis is very long, one is intermediate and the third is rarely measurable because the blebs are paper thin, ...their original shape is unknown and the may indicate slickensides in cleavage surfaces..." (Cloos, 1971, p. 45.). In the study area the axes of the chlorite amygdules were easily measured and not "paper thin", contrasting with those studied by Cloos. The relationships between the macroscopic features are illustrated in Figure 4.

ii) General Microscopic Features:

The principal minerals within the groundmass include albite, chlorite, epidote, actinolite and sphene with minor amounts of hematite and possibly pyroxene. All specimens show effects of shearing and primary textures are obliterated. Reed (1955) describes relict textures of Catoctin Volcanics near Luray, Virginia in rocks which are not sheared to the same degree as in South Mountain study area. The original textures however were undoubtedly similiar.

FIG. 4 South Mountain deformation plan. Shows fanning regional cleavage, bedding and lineations in "a" normal to "b". Lineation is recognized on the cleavage surface. (from Cloos 1951b)

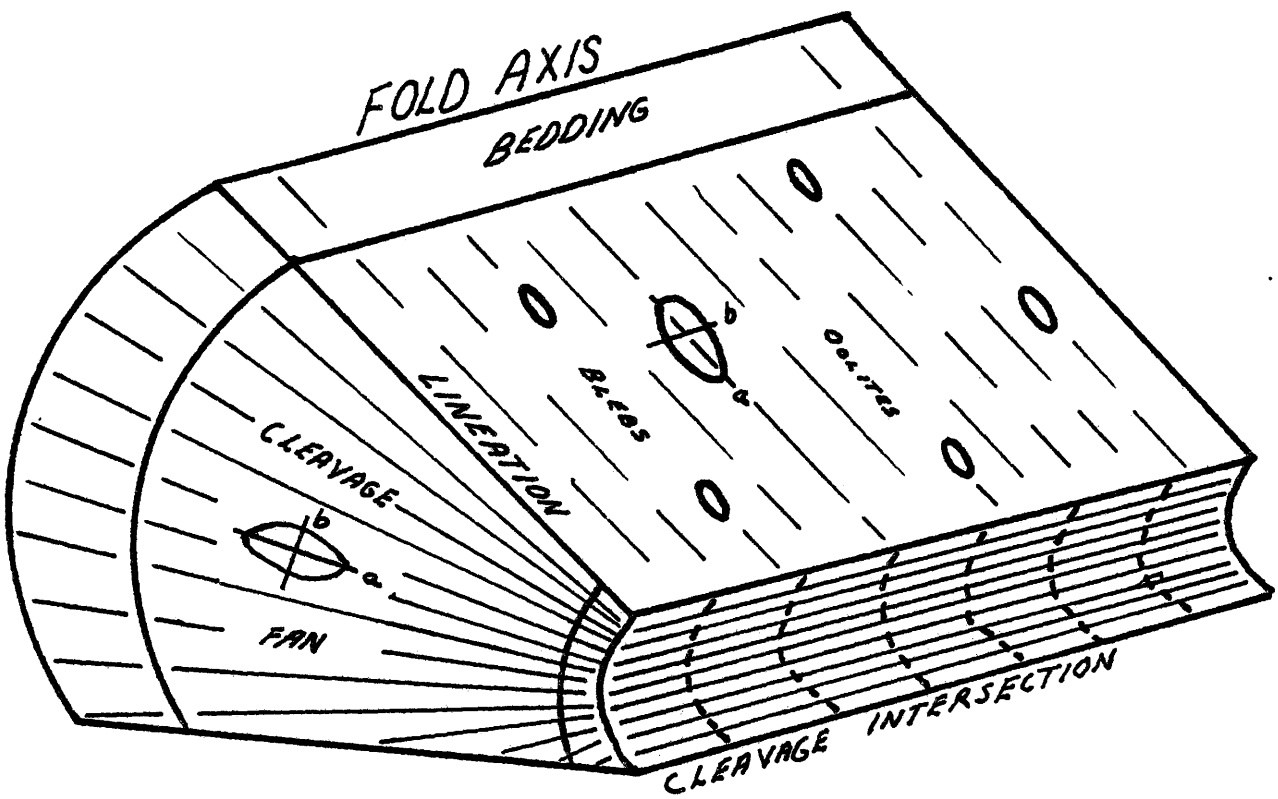

Reed (1955) states that, ..."where the greenstones are not sheared the texture is that of the original lava. The rock consists of interlocking plagioclase laths (now albite) in an interstitial matrix of chlorite, actinolite, epidote, sphene, leucoxene, and magnetite. Original pyroxene grains are common between the laths in some specimens, but in most of the finer grained rocks the pyroxene is almost completely altered. This texture suggests the typical basaltic texture in which the spaces between the plagioclase are filled with either granular crystals of pyroxenes (intergranular) or basalt glass (interstitial). The present texture of the greenstone is probably the result of alteration of the interstitial fillings between plagioclase laths to secondary minerals. Large irregular patches of chlorite are fairly common in the greenstone and some resemble the chlorophaeite patches of fresh basalts .... in most greenstones the groundmass plagioclase laths average about .05 by .4 mm., plagioclase phenocrysts in the porphyritic flows generally average less than one cm. in length ..." (Reed, 1955, p. 888.). The important point to note is the similiarity of the texture to that of a basalt (random orientation of minerals). Presumably it is this texture which is to be modified. Microscopic examination reveals two distinct populations of amygdules within greenstone, chlorite rich and epidote

rich. The chlorite rich amygdules are commonly "rimmed" by epidote grains and are generally elliptical in thin section. Epidote amygdules contain small amounts of chlorite and are circular in thin section. These two populations will be discussed further in Chapter 3. Amygdules within the epidote lenses are commonly filled with epidote or quartz and are sub-circular.

iii) Depositional Environment of Volcanics:

There are two theories concerning the nature of the emplacement of the volcanics, 1) they are sub-aerial tholeiitic basalts extruded through fissures as in the Columbia Plateau (Reed, 1955) or 2) they are sub-aqueous spilites (Stose and Stose, 1946; Whitaker, 1956). The evidence in support of option one includes : 1) the absence of pillow structures 2) lack of evidence of any central chain of volcanoes 3) absence of large masses of greywackes and bedded cherts 4) the presence of "feeder" dykes of Catoctin composition 5) presence of pigeonite and 6) columnar jointing. Evidence supporting option two include: 1) spilitic mineralogy and chemical composition 2) high soda content 3) presence of thin sedimentary interlayers and 4) association of volcanics with thick sequences of eugeosynclinal sediments in the south-east section of the Blue Ridge (Bloomer, 1950; Bloomer and Werner, 1955).

The evidence appears to indicate sub-aqueous deposition on the south-east side of the Blue Ridge and a sub-aerial tholeiitic basalt emplacement in the north-west side (South Mountain).

1v) Metamorphism:

The volcanics were subjected to metamorphism in mid- Paleozoic time. This low temperature and pressure (350°C, 3.5 Kbar) (Mitra, 1978) event appears to have been concurrent with cleavage development and lineation during formation of the Blue Ridge (Cloos, 1957, 1968). The metamorphic grade increases to the south-east.

CHAPTER III

STRUCTURAL ANALYSIS AND MICROSTRUCTURES

1. DETERMINATION OF THE ORIGINAL SHAPE OF DEFORMED AMYGDULES

Several methods were used to determine the original shape of the amygdules. Studies in similiar basalts (Columbia-Snake and Deccan Plateaus) indicate flow top amygdules are initially near- spherical. Minor tectonic events may alter this initial sphericity before final deformation took place; therefore justifying the examination of initial shapes. The three methods employed are outlined below along with their respective results.

Ramsay (1967) proposed the application of the equation $Ro=(Rfmax./Rfmin.)^{\frac{1}{2}}$ to points located on flucuation plot (Rf vs $\emptyset$). The equation was applied to the fluctuation plots constructed for amygdules on each of the three mutually perpendicular specimen faces (Figures 5-10). The equation is applicable to amygdules which are initially randomly oriented and inequant. Results indicate original axial ratios of 1.445:1:.55 (Measurements of specimens 1 and 2; excluding epidote rich amygdules) and 1.49:1:.54 (for all amygdules).

Figure 5. Fluctuation plot of chlorite amygdules on the XY plane of specimen 1.

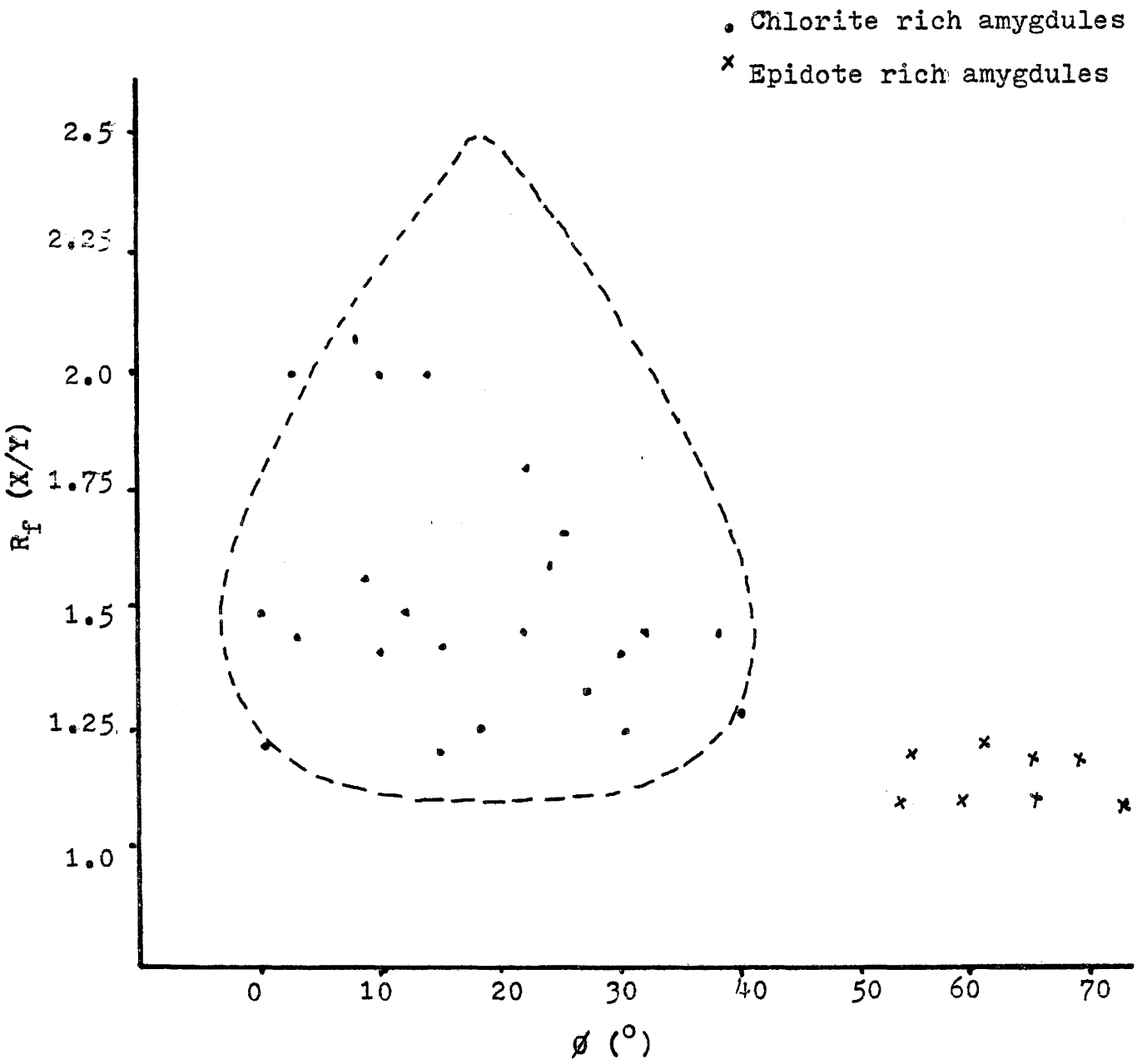

Figure 6. Fluctuation plot of chlorite amygdules on the XZ plane of specimen 1.

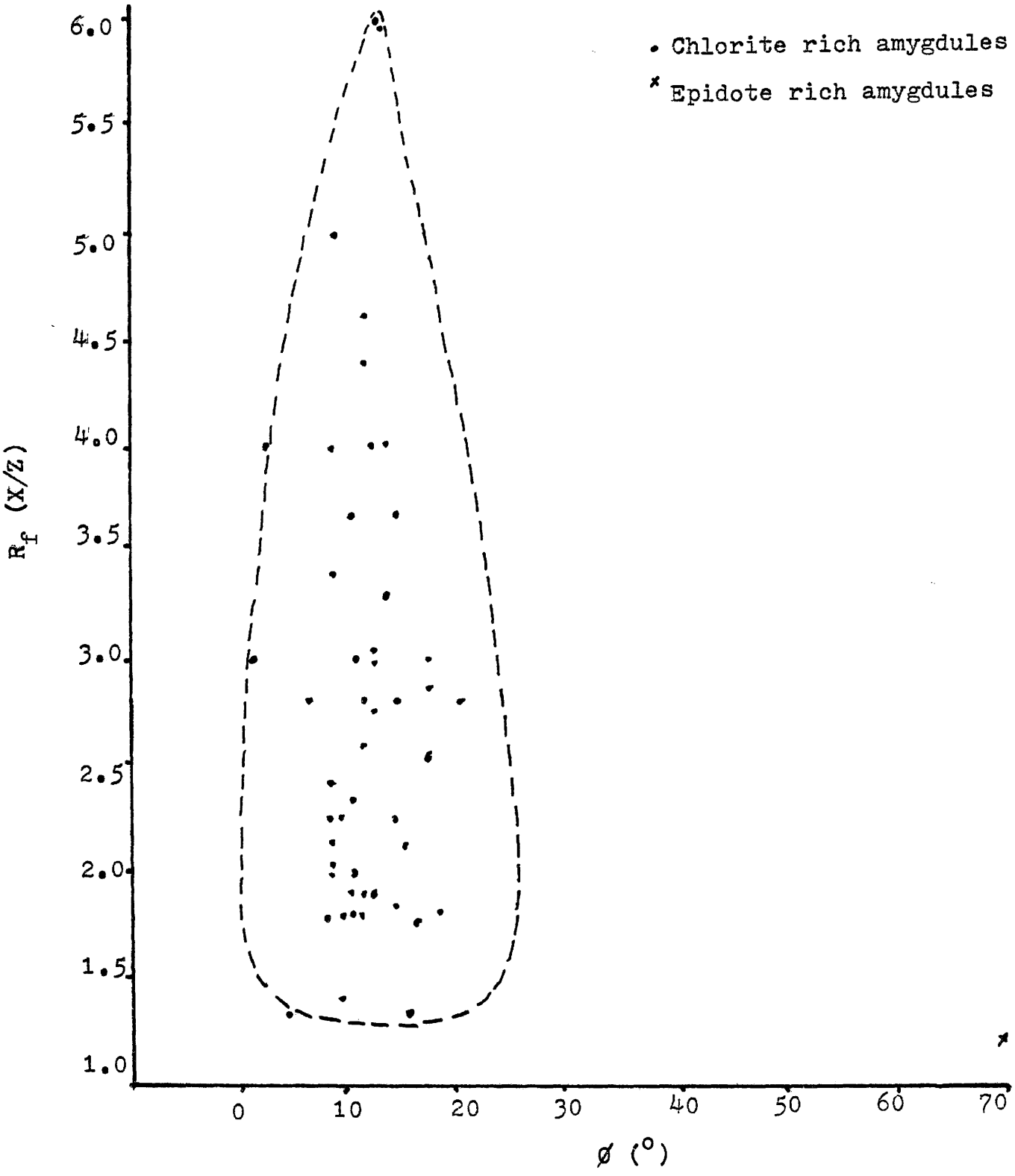

Figure 7. Fluctuation plot of chlorite amygdules on the YZ plane of specimen 1.

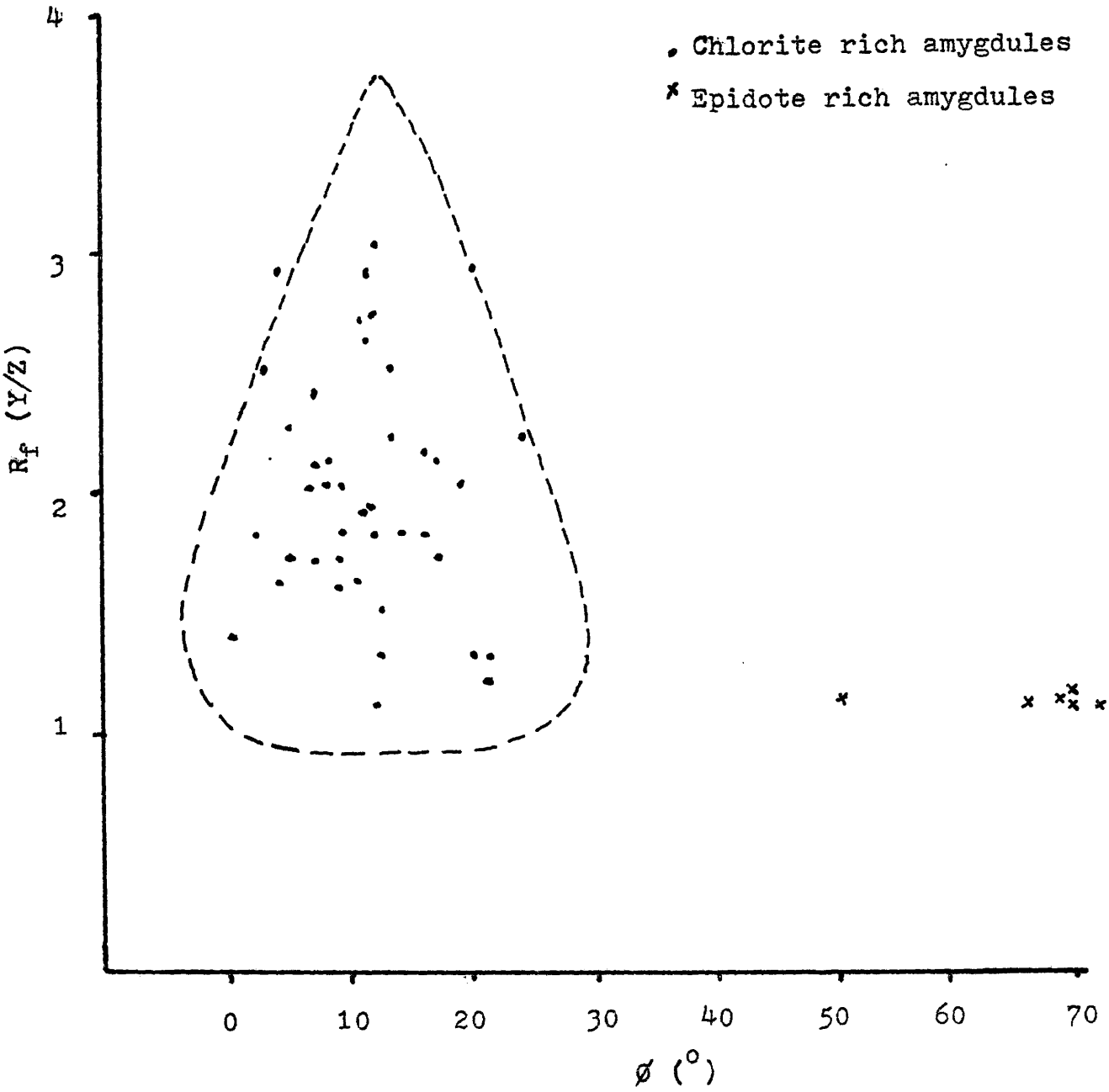

Figure 8. Fluctuation plot of chlorite amygdules on the XY plane of specimen 2.

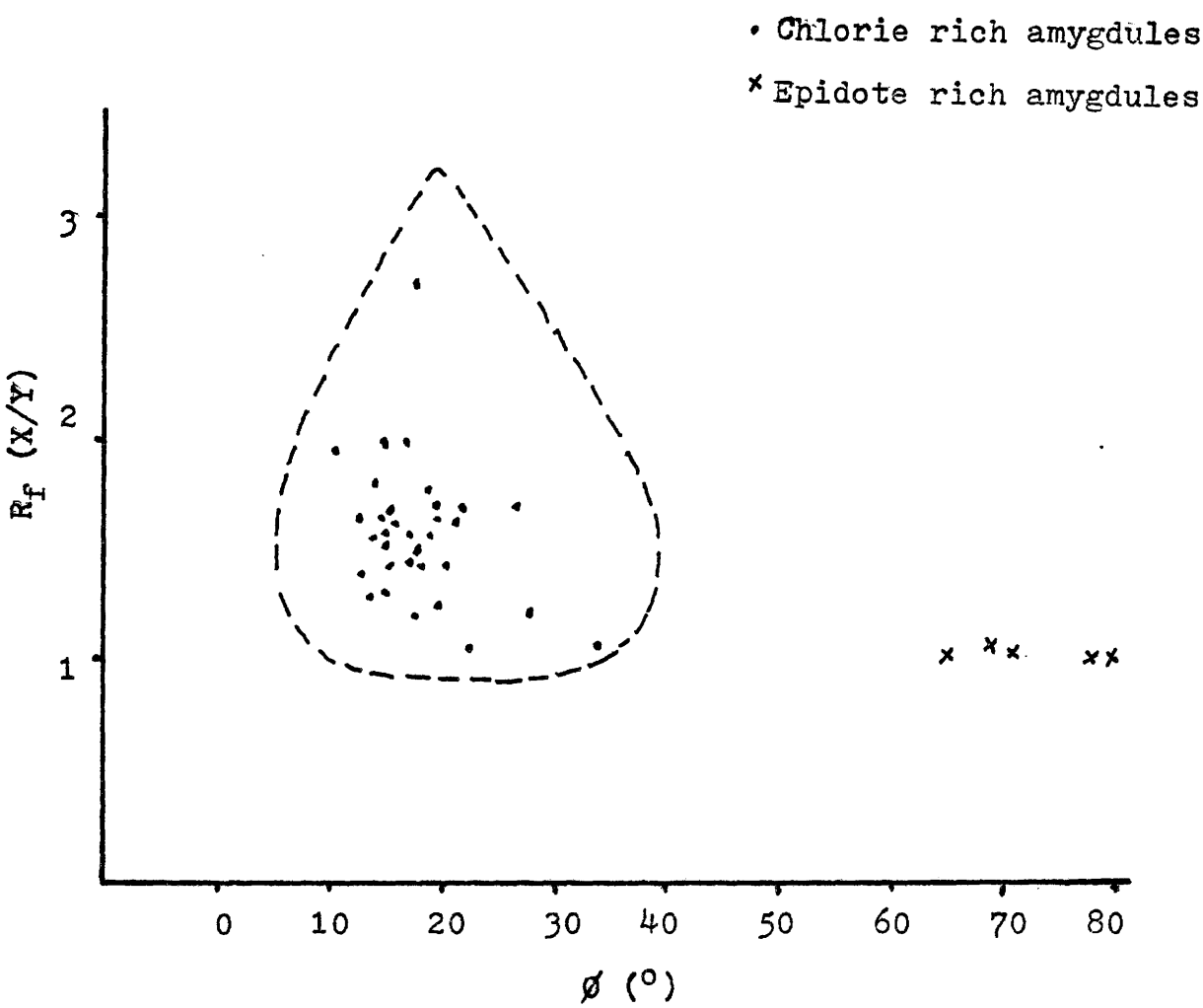

Figure 9. Fluctuation plot of chlorite amygdules on the XZ plane of specimen 2.

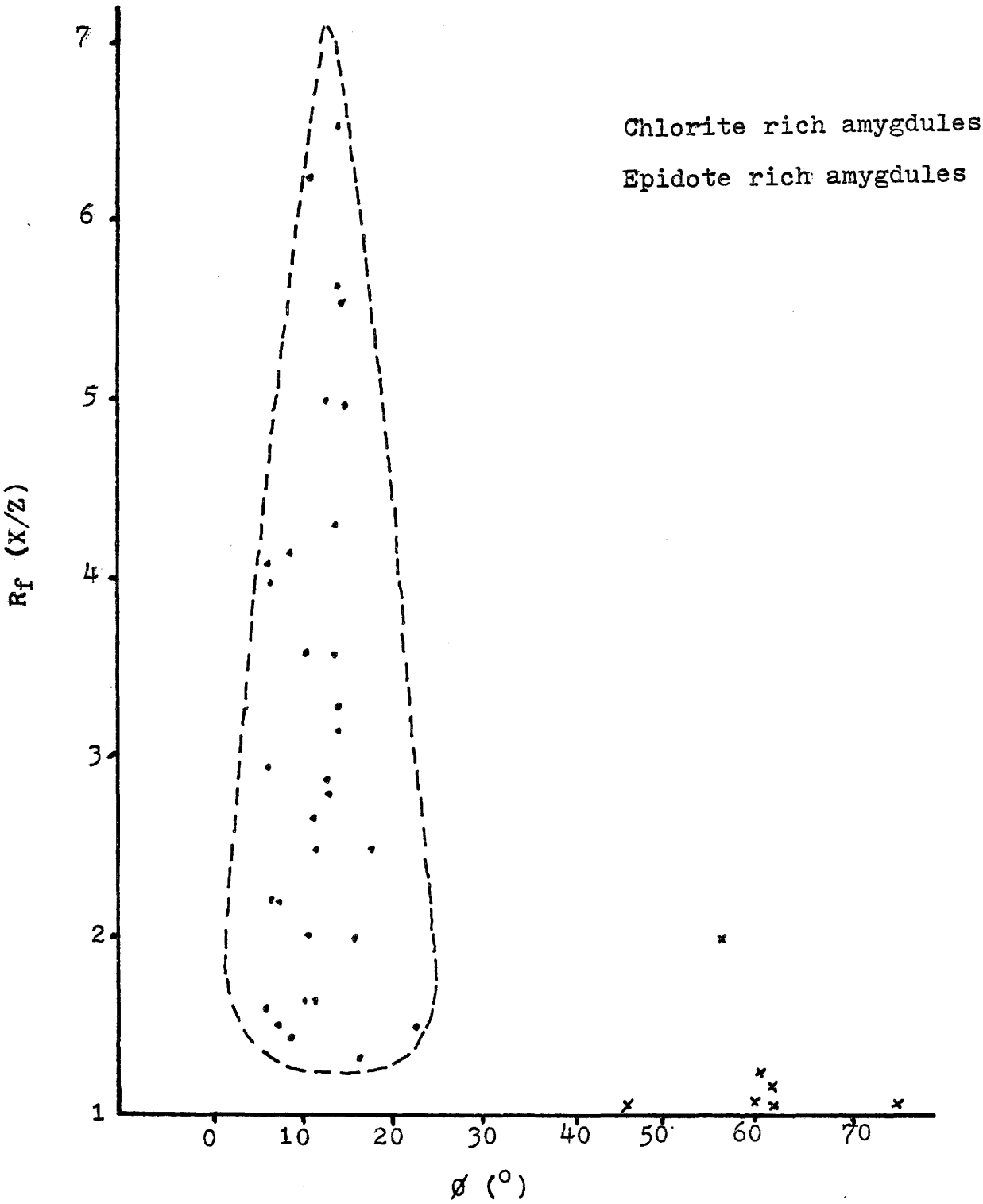

Figure 10. Fluctuation plot of chlorite amygdules on the YZ plane of specimen 2.

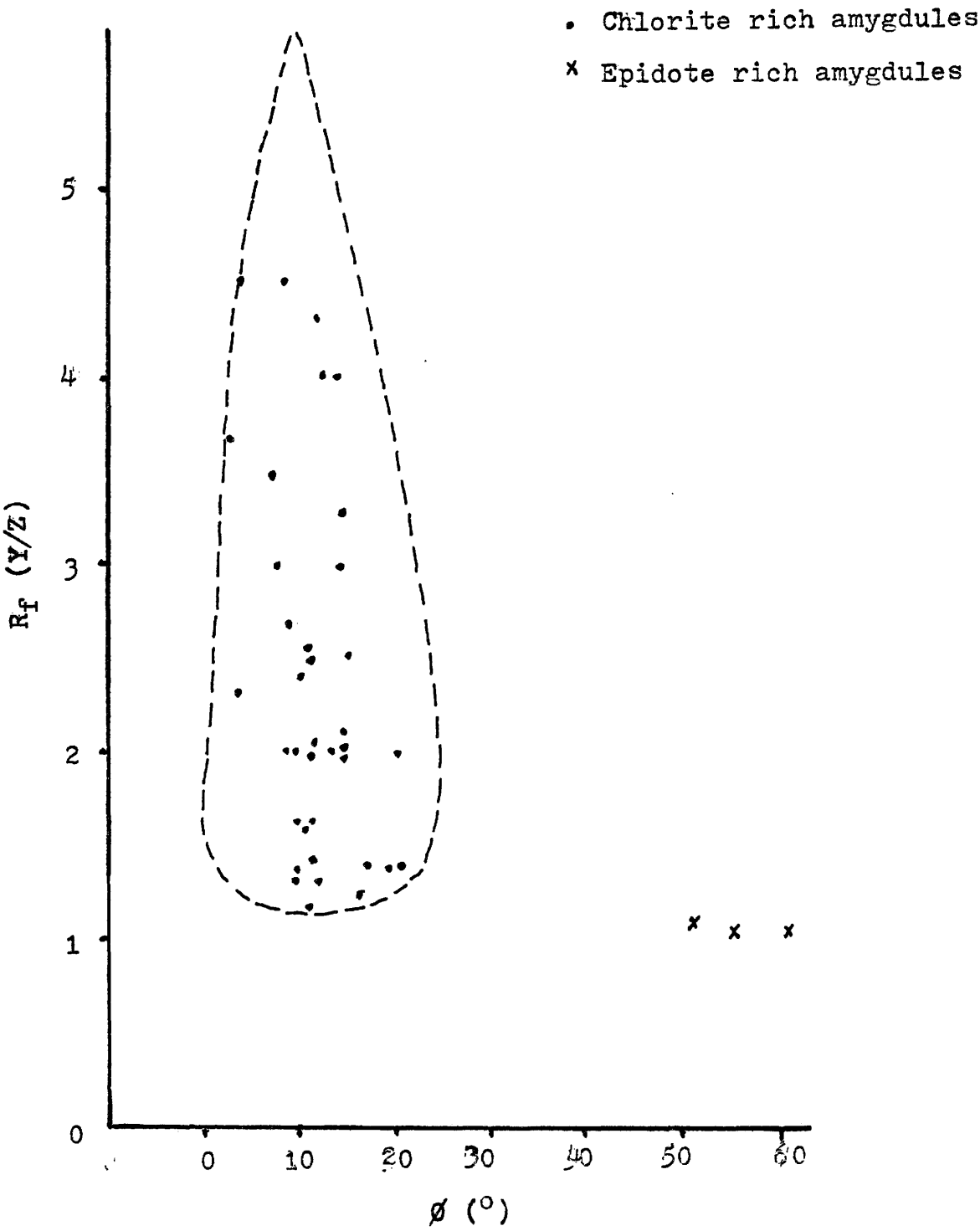

Hsu (1970) used a modified fluctuation plot in which the calculated ϕ_c value representing the symmetry line for the bell-shaped distribution of points is located at X=0 (Figures 11 and 12). All points with ϕ less than ϕ_c are reflected about the ordinate axis. Two isostrain curves are constructed representing the maximum and minimum strain values to which the amygdules were subjected. The resultant intercepts obtained from the intersection of the isostrain curves and the coordinate axes are subsequently substituted into equations:

R_tR_o=point of intersection of outer curve and the axes $\phi=0^o$

R_o/R_t=point of intersection of outer curve and the axes $\phi=90^o$

and R_oR_t =point (of largest value) of intersection of inner curve and the $\phi=0^o$ axes

R_t/R_o=point (of smallest value of intersection of inner curve and the $\phi=0^o$ axes

Solving simultaneously the resultant R_o is found (for the XY plane of specimens 1 and 2) to be 1.54:1.

The final method is that of Wood (1974). It involves the construction of a deformation plot which records the change in the principal axial ratio of the amygdules from the original (pre-deformation) state through to the final principal axial ratios. Details of construction are found later in the

Figure 11. Construction of the bounding isostrain from the fluctuation plot for the XY plane of specimen 1.

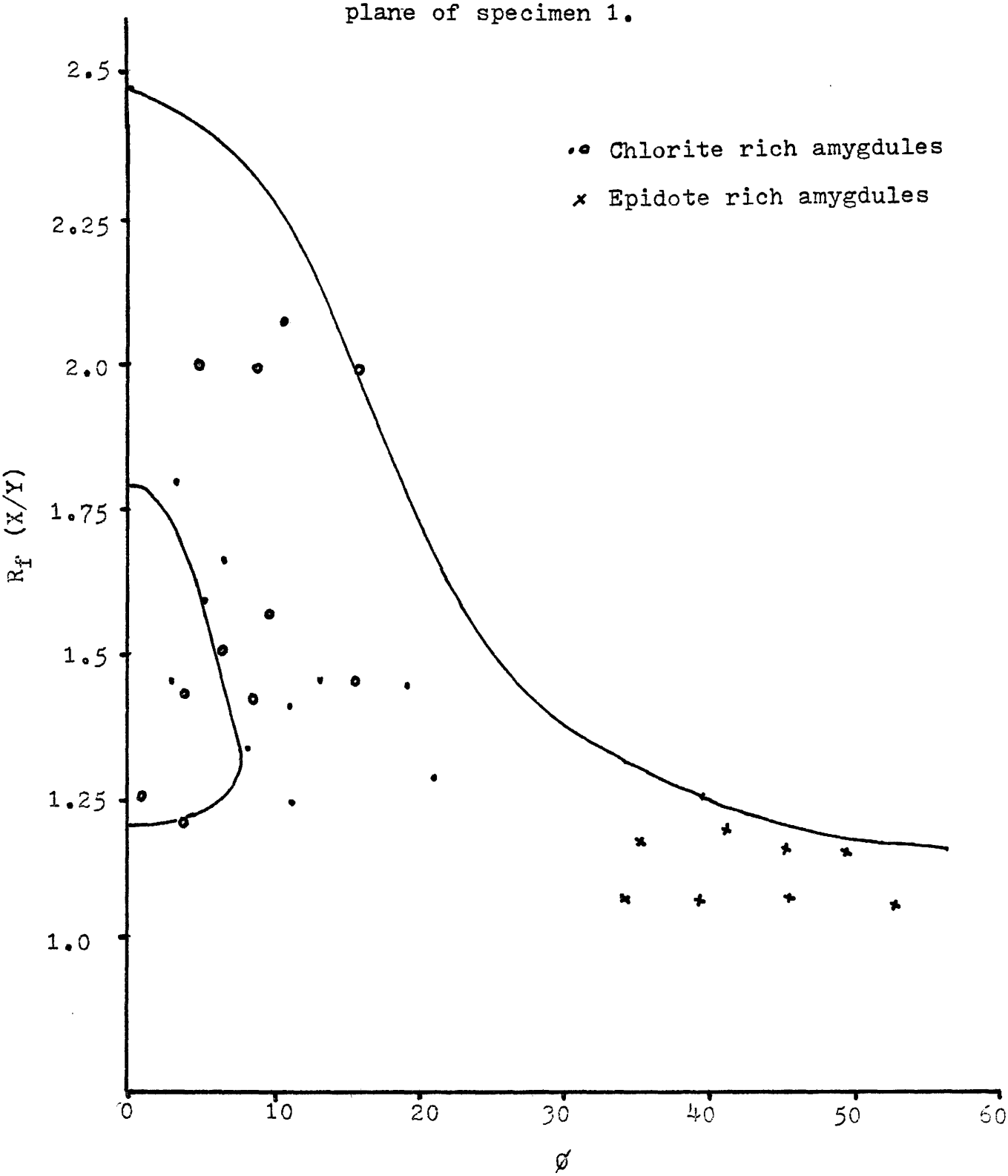

Figure 12. Construction of the bounding isostrain curves from the fluctuation plot for the XY plane of specimen 2.

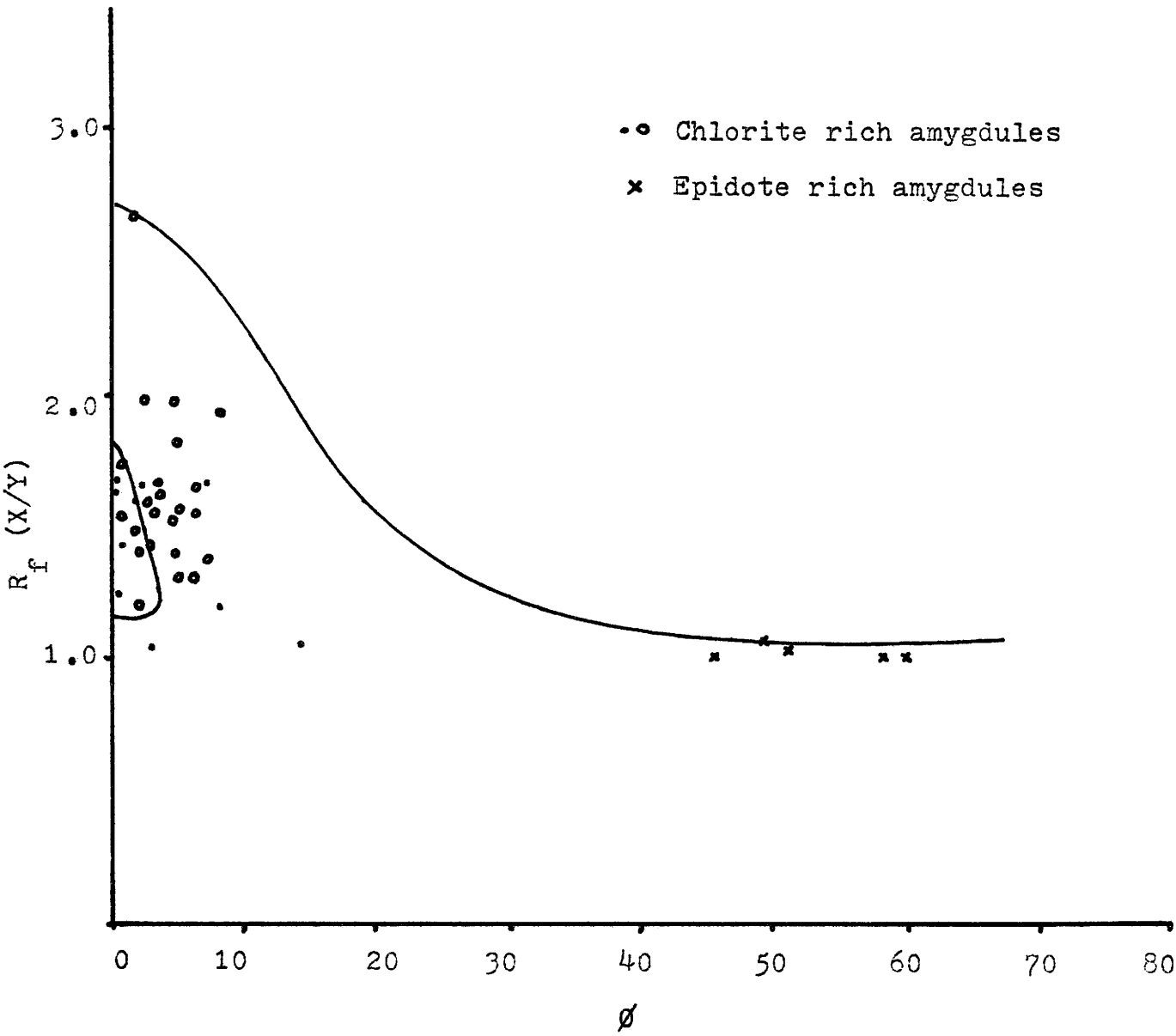

chapter (Figures 16 and 20). Estimation of the original principal (X/Y) axial ratio is 1.25:1 (excluding the epidote rich amygdules).

The results of the three previous methods indicate that the initial shape (immediately before deformation) of the amygdules was not spherical. This non-sphericity may be due to: i) original elongation at the time of emplacement due to lava flowage, ii) the effect of a previous deformation or iii) a period of initial flattening, perhaps a result of stress applied by overlying strata or by lateral flowage and vertical shortening (axially symmetric). The results are quite encouraging since the two primary methods (those of Ramsay and Hsu) designed specifically for this purpose do show similiar results (1.45:1 versus 1.54:1). The author feels the use of Wood's deformation path could be useful in determining the initial shape of the amygdules and the resultant 1.24:1 value does not diverge greatly from the other values.

2. DETERMINATION OF THE TECTONIC STRAIN ELLIPSOID AND ORIENTATION OF THE PRINCIPAL AXES

Two methods were employed to estimate the nature of the tectonic strain ellipsoid: That of Ramsay (1967) and Hsu (1970).

The basis of Ramsay's method is the equation $R_t=(Rfmax. Rfmin.)^{\frac{1}{2}}$, where Rfmax. and Rfmin. values are taken from the fluctuation plot. The R_t values were established for amygdules on all three mutually perpendicular "faces" (Figures 5-10). The resultant tectonic strain ellipsoids have principal axial ratios 1.655:1:.488 (excluding epidote rich amygdules) and 1.6:1:.5 (including epidote rich amygdules).

Hsu's method is identical to that described previously for determination of R_o. Results for (X/Y) principal axial ratio indicate 1.68:1 and 1.52:1 for specimens 1 and 2 respectively and 1.6:1 as an average for both specimens.

It appears that both methods produce similiar results. The means of the axial ratios of amygdules on the three perpendicular faces resulted in a tectonic strain ellipsoid of dimension 1.48:1:.493 for specimen 1 and 1.57:1:.535 for specimen 2. These values correspond well to those derived from the previous methods.

The method employed to obtained the "mean" orientation of the long axes of amygdules (on the three faces) was taken from Ramsay (1967). Theoretically when a rock is deformed homogeneously (when $R_t>R_o$) the plot of Rf vs ϕ (ϕ for initially randomly arranged strain markers) will form a symmetrical, bell-shaped configuration.The axis of symmetry of this distribution ideally represents the orientation of the greater

principal stress for the section of measurement.

Results can be read directly from the fluctuation plots for each section (Figures 5-10). The orientations of X, Y and Z (the principal axes of the tectonic strain ellipsoid; they are mutually perpendicular linear elements) are approximately 127/57°E, 217/11°S, and 317/33°W respectively (Figure 21).

Inspection of individual fluctuation plots reveals:

i) The range of fluctuation angles for identical faces in specimens 1 and 2 are remarkable similiar.

ii) The amygdules within the XZ plane contain the highest Rf values and the smallest range in fluctuation angle of any face.

iii) The amygdules within the XY plane have the lowest Rf values and largest range in fluctuation angle.

There is a clear relationship between the amount of strain and the angular deviations of long axis orientation from the direction of the principle stress.

These orientation results can be readily obtained merely from observation in the field without great error since the lineation orientation appears constant and the size of the amygdules permits easy recognition.

3. CONSTRUCTION OF A DEFORMATION PATH

Generally reconstruction of a deformation path is difficult (particularily when large study areas are involved) due largely to the strain heterogeniety encountered. This strain heterogeniety may be a result of variation in rigidity

Figure 21. Stereonet illustrating orientations of various features

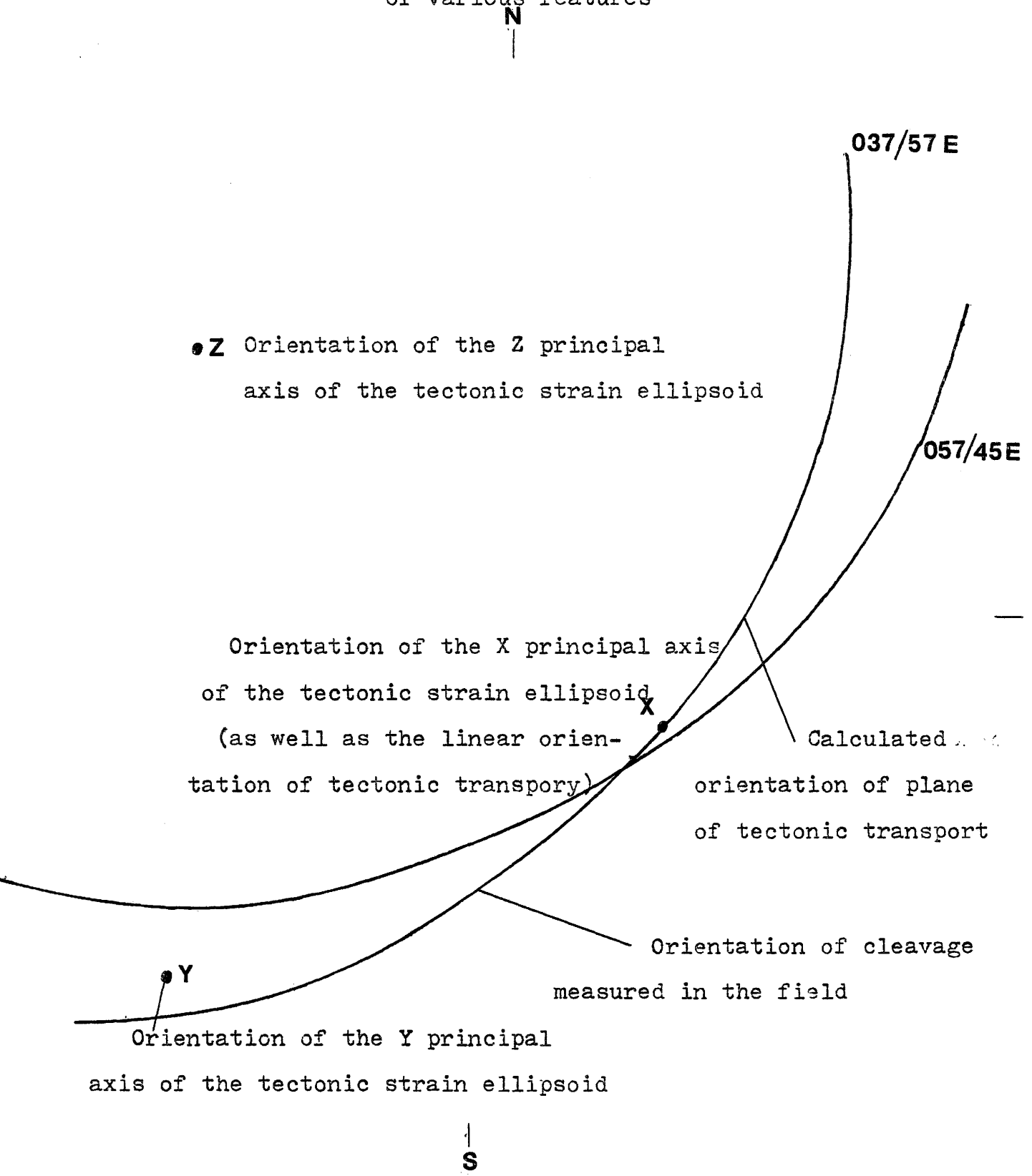

of amygdules (due to different proportions of minerals ie. epidote and chlorite), size variations of amygdules, and perhaps slight variation in groundmass ductility. The method employed is described in detail by Wood (1974, 391-392). Wood assumes that the strain is homogeneous at the scale one is working at. This condition is satisfied since the size of block used is fairly small (4 cm. x 3 cm.) and separate measurements including only amygdules rich in chlorite were made. The method is very simple and outlined below:

i) The axial ratios of the amygdules for the XY, ZY or XZ planes are ranked in order from highest to lowest.

ii) The ratios are grouped so that 20% of the total number of ratios are within each group.

iii) The means are computed for each of the five groups.

iv) The corresponding ordered pairs for each group are plotted graphically (arithmatic scale). The line connecting these points is the deformation path.

The histograms as well as the deformation paths are illustrated for both specimens (Figures 13-20). The deformation paths are also plotted on a logarithmic plot which provides a better understanding as to the mode of deformation than does Wood's arithmetic scale (Figures 22 and 23).

Examination of Figures 20, 22, and 23 strongly

FIG.13 Histogram illustrating the variation of the X/Y axial ratios for the chlorite blebs on the XY plane of specimen # 1.

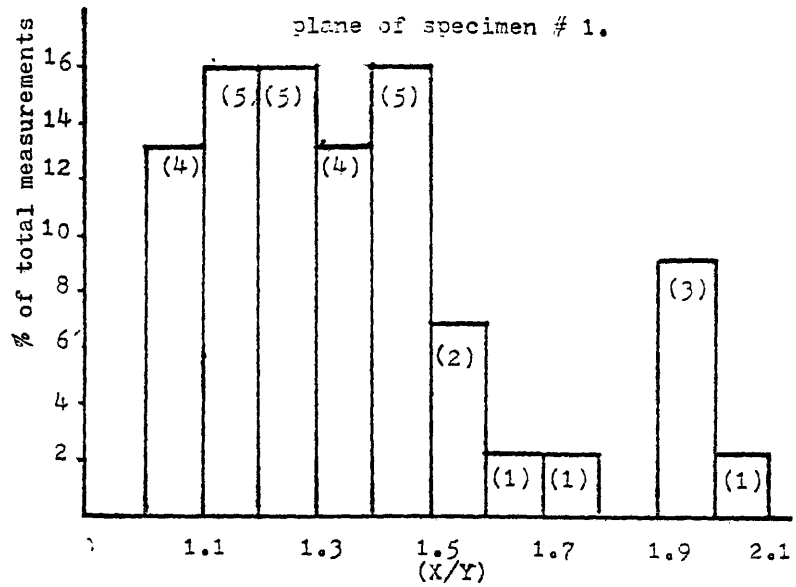

FIG.14 Histogram illustrating the variation of the Z/Y axial ratios for chlorite blebs on the YZ plane of specimen # 1.

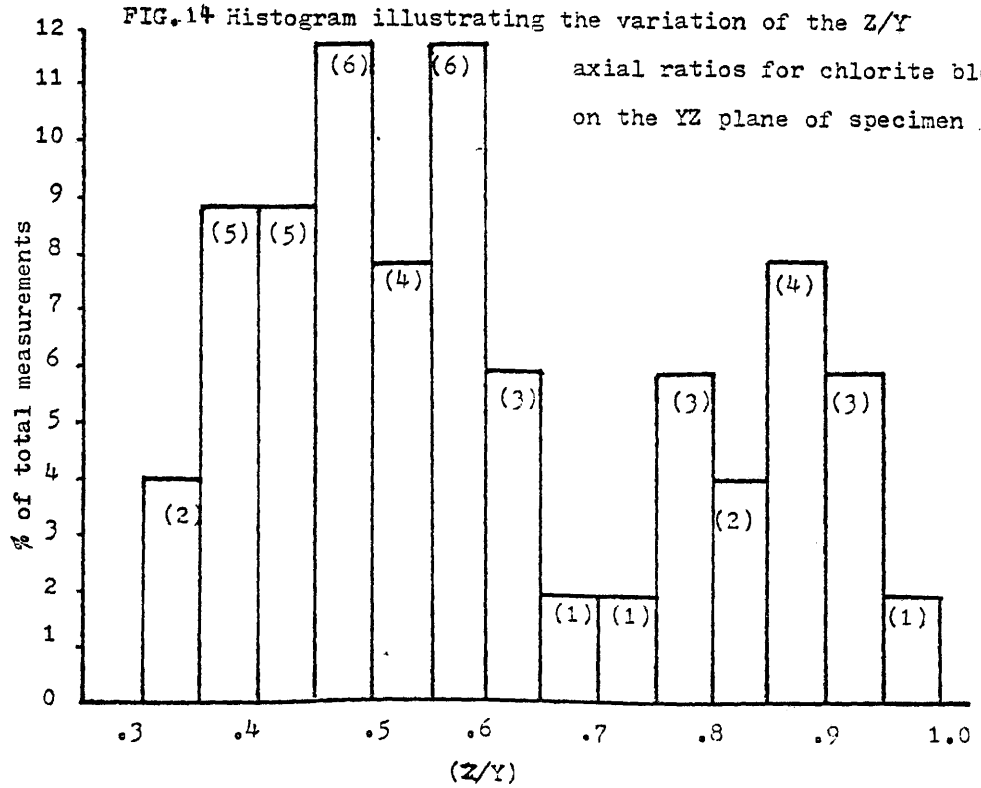

FIG. 15 Histogram illustrating the variation of the X/Z axial ratios for chlorite blebs on the XZ plane of specimen #1.

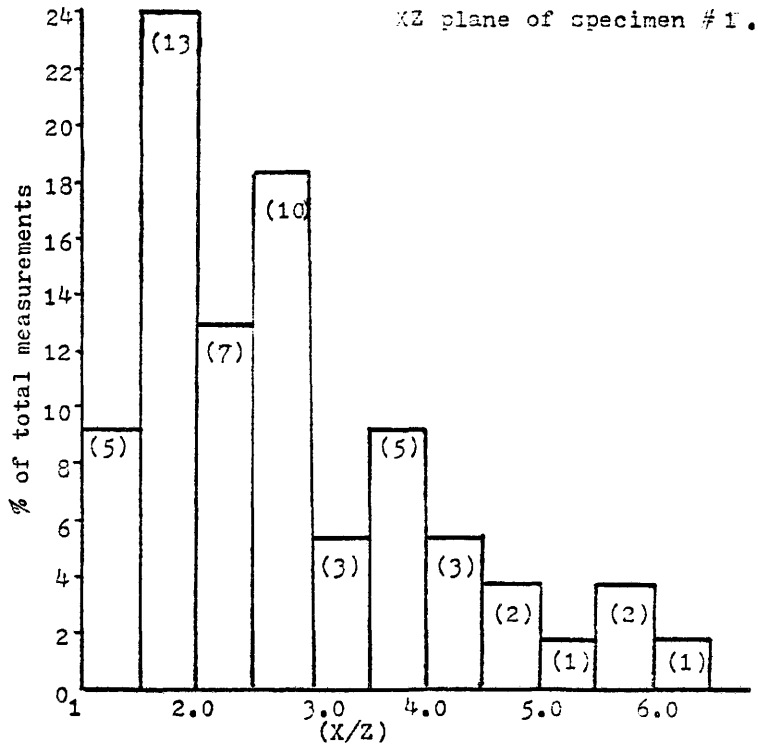

FIG. 16 Deformation plot with curve of plane strain at constant volume and deformation path predicted from strain heterogeneity. (For specimen #1.)

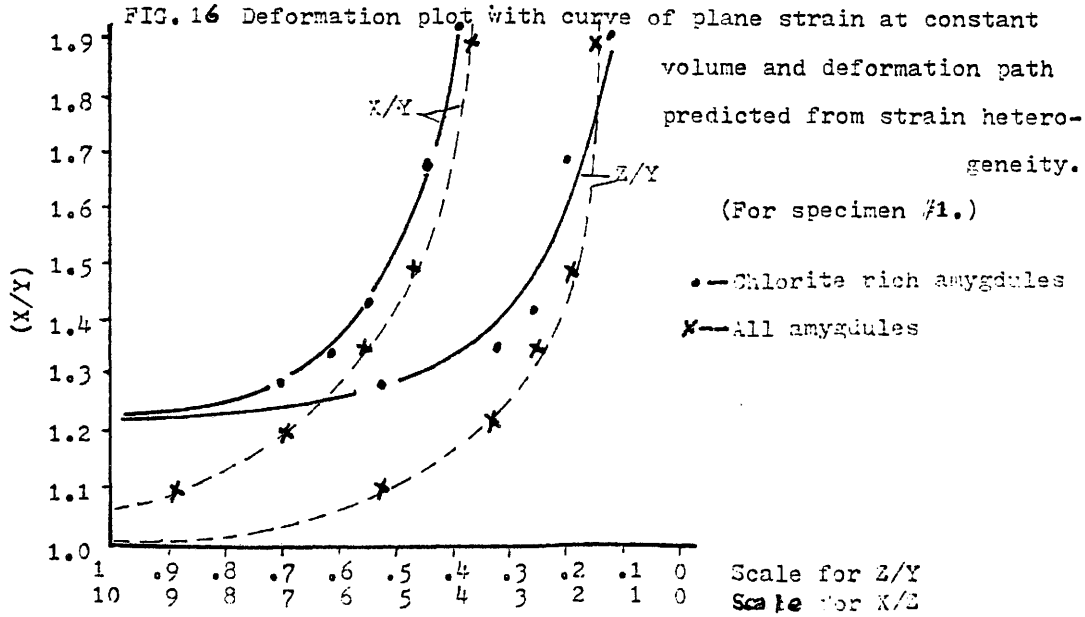

FIG. 17 Histogram illustrating the variation of the X/Y axial ratios for the chlorite blebs on the XY plane of specimen # 2.

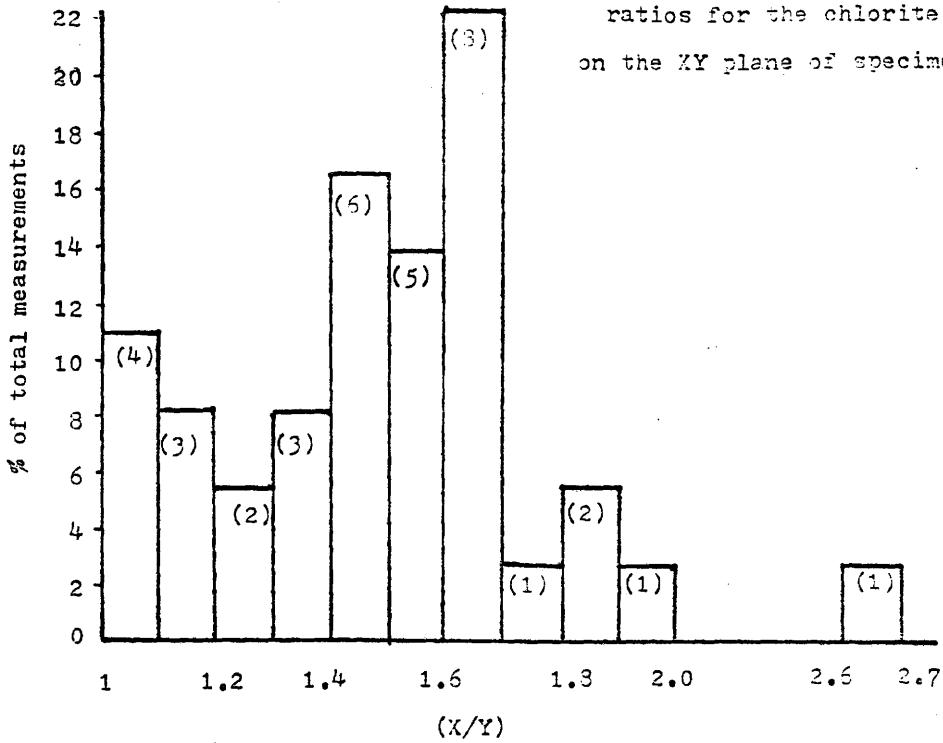

FIG. 18 Histogram illustrating the variation of the Z/Y axial ratios for chlorite blebs on the YZ plane of specimen # 2.

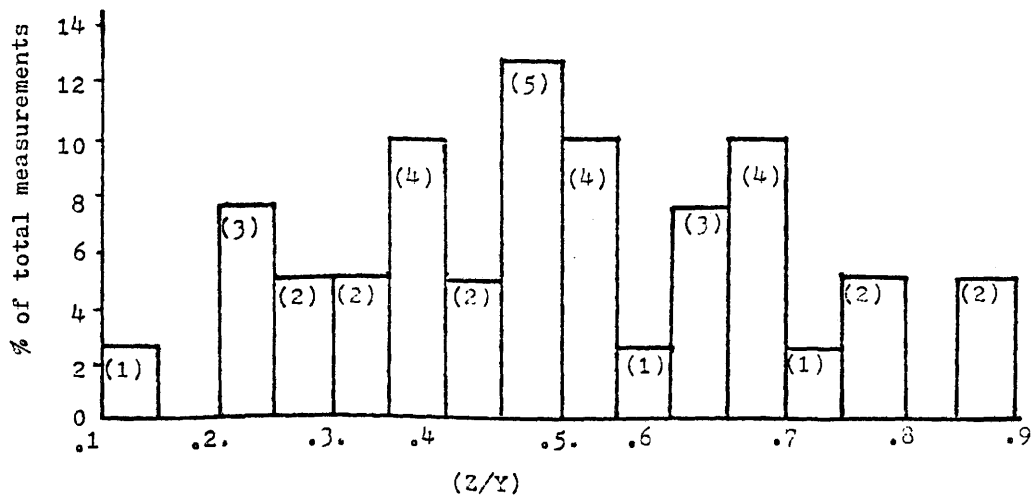

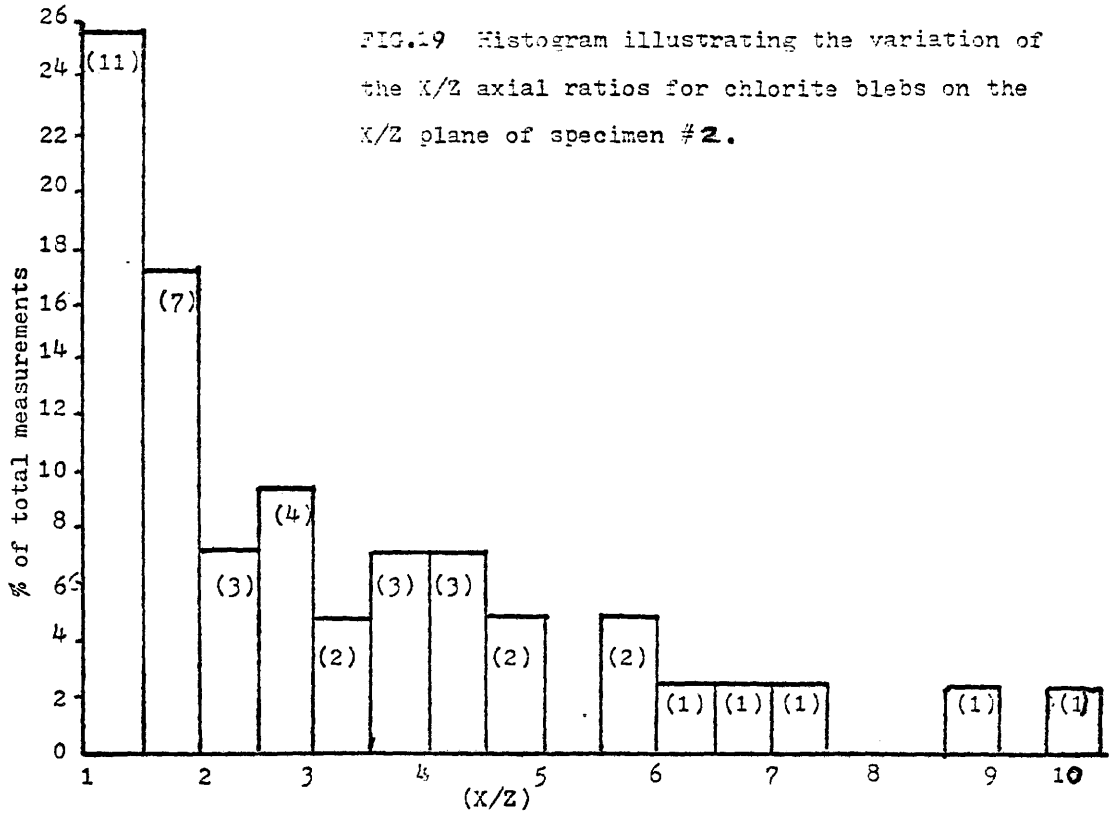

FIG.19 Histogram illustrating the variation of the X/Z axial ratios for chlorite blebs on the X/Z plane of specimen #2.

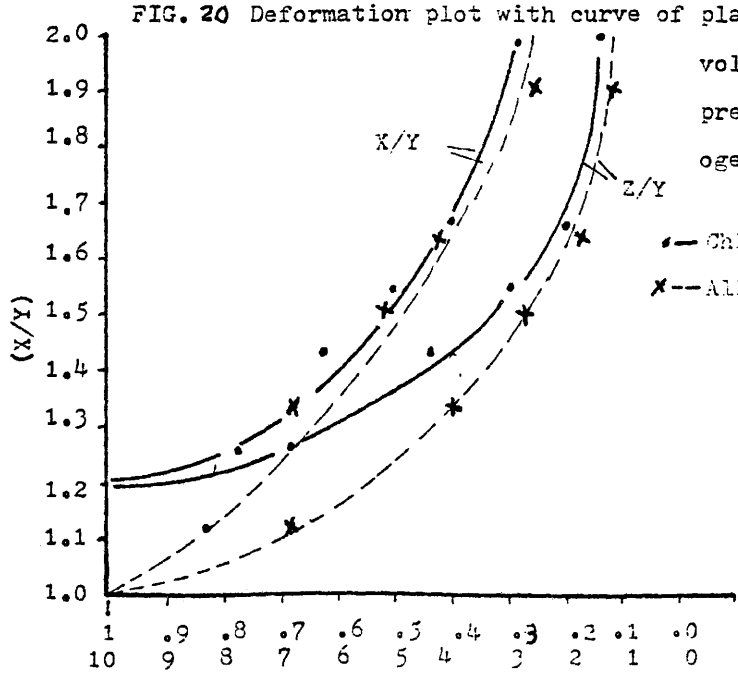

FIG. 20 Deformation plot with curve of plane strain at constant volume and deformation path predicted from strain heterogeneity. (for specimen #2.)

Figure 22

Logarithmic deformation plot showing the deformation path for amygdules (both chlorite and epidote rich) in specimens 1 and 2.

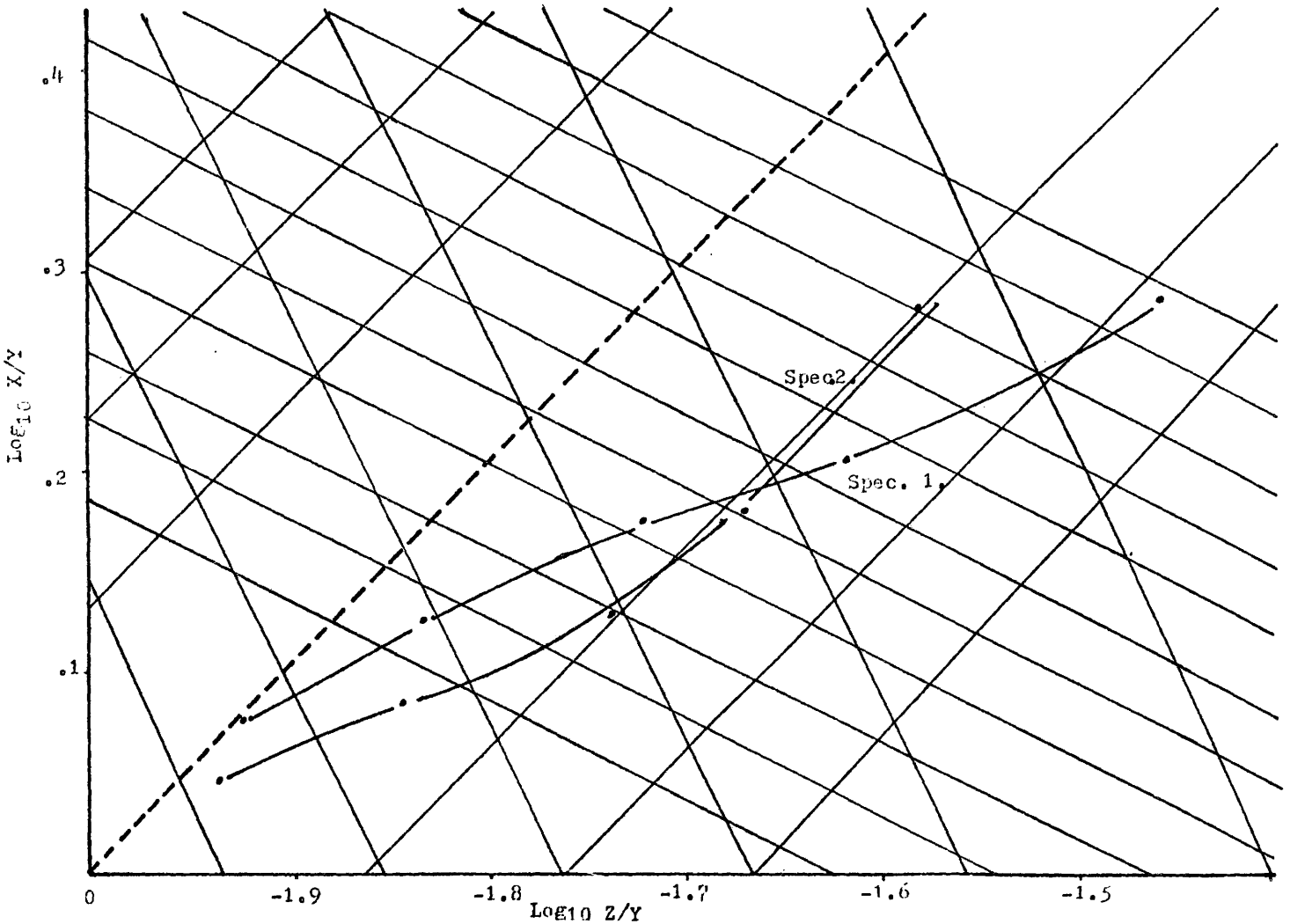
.4
.3
.2
.1
Log_{10} X/Y
Spec2.
Spec. 1.
0
-1.9
-1.8
-1.7
-1.6
-1.5
Log_{10} Z/Y

Figure 23

Logarithmic deformation plot showing the deformation path for amygdules (chlorite rich only!) in specimens 1 and 2.

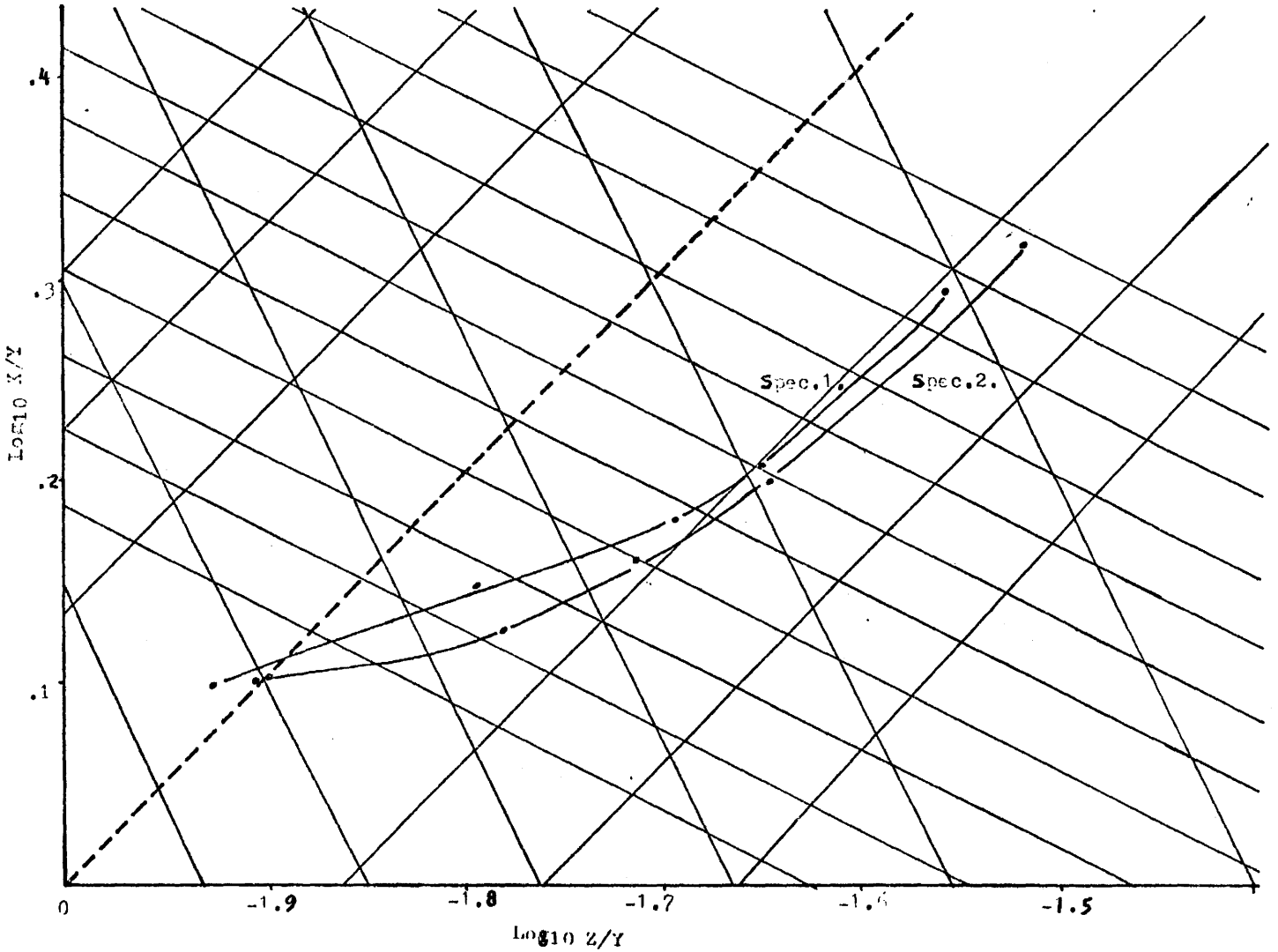
.4
.3
.2
.1
0
-1.9
-1.8
-1.7
-1.6
-1.5
Log10 X/Y
Log10 Z/Y
Spec.1.
Spec.2.

suggest an initial stage of amygdule flattening followed by plane strain (this is best seen on the logarithmic plot as well as the Flinn Diagram) (Figure 24). In fact this initial flattening may well be responsible for the calculated 1.45:1:.55 axial ratios for the original undeformed amygdules. Comparison of specimens indicate that amygdules from specimen 2 suffered a greater degree of plane strain than those of specimen 1, yet an equal amount of flattening, perhaps due to stresses applied by overlying sediments should be fairly constant between locations only five metres apart, as were specimens 1 and 2. Thus the intensity of plane strain must have varied locally.

4. MICROSTRUCTURES

Microstructures within amygdules, at amygdule-groundmass contacts, within the groundmass and behaviour of amygdules and cleavage aid in the evaluation of the development of specific structures and the deformation as a whole.

i) Microstructures Found Within Amygdules:

Two distinct populations of amygdules can be identified on the basis of i) mineralogy (proportion of chlorite vs. epidote) ii) structural analysis (previously discussed) and iii) microstructures. The chlorite rich and epidote rich amygdules will be discussed separately.

Figure 24. Flinn Diagram illustrating the deformation path of specimens 1 and 2 combined.

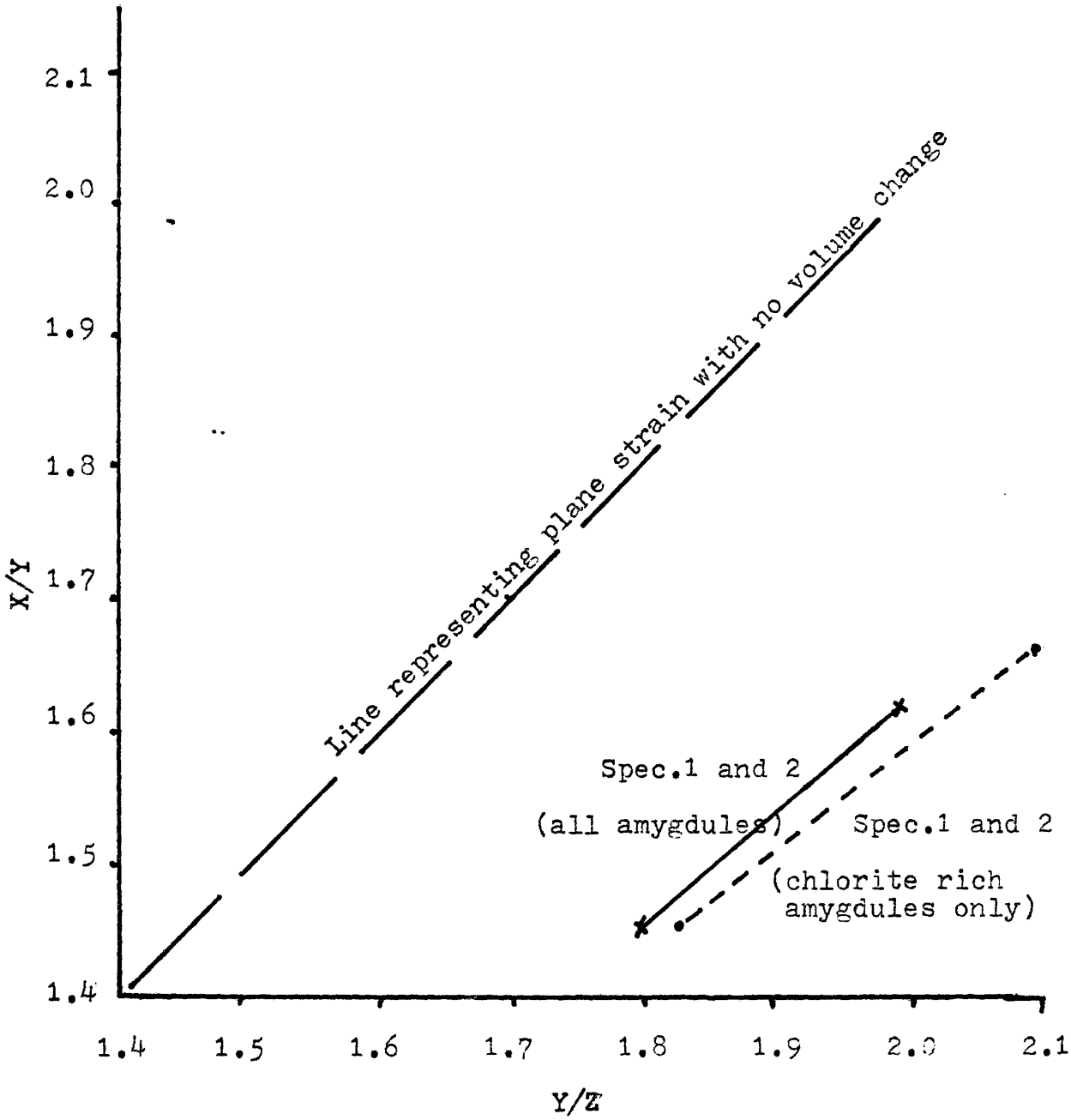

a) Chlorite rich amygdules. The microstructures found within these amygdules prove to be very useful in determination of the nature of development of structures.

Chlorite appears in two distinct domains within the amygdules: i) Domain 1 which is characterized by fan shaped chlorite aggregates and represents the early schistosity (Plate 3A). and ii) Domain 2 characterized by elongate well oriented chlorite grains and which will be referred to as the crenulation cleavage (Plates 1B and 3A).

The fan shaped chlorite is found predominantly in"protected" areas surrounded by epidote,and to a lesser extent between layers of crenulation cleavage and adjacent to the amygdule walls (Plates 4A and 4B). This early schistosity is oriented at high angles (60-70°) to the crenulation cleavage.

The elongate chlorite representing the crenulation cleavage is common in amygdules with high aspect ratios in the XZ plane; particularly those with minor amounts of epidote. A definite correlation exists between the aspect ratio (shown by the amygdules within the XZ plane) and the degree of domainal development. Inspection of numerous amygdules reveals a continuum, from essentially a random chlorite fabric in sub-circular amygdules, to the development of a domainal fabric consisting of a crenulation cleavage and an early schistosity, to a single domain fabric consisting entirely of crenulation within amygdules of high aspect ratio (5:1). Plates 1 through 3

Plate 1

(A) Random fabric in chlorite rich amygdule of low aspect ratio (XZ) plane. Individual chlorite grains (sc) are commonly short and stubby. Bar scale = .28 mm.

(B) Two varieties of chlorite grains in an amygdule of moderately low aspect ratio in the XZ plane. The fan shaped chlorite aggregate (fc) is clearly oriented at a high angle to the elongate chlorite grain (ec). A crude alignment of elongate chlorite grains is evident, however this is on an individual scale and no domainal fabric is visible. The adjacent grain is epidote (ep) Bar scale = .18 mm.

A

B

Plate 2

(A) Small grains of elongate chlorite (ec) are aligned around the large fan shaped chlorite aggregate (fc). Note that this alignment rapidly dissipates away from the contact with the fan shaped aggregate (fc). The alignment is discontinuous throughout the amygdule and is only visible when in contact with chlorite aggregates. Bar scale = .17 mm.

(B) The elongate chlorite grains (ec) alignment shows greater continuity throughout the entire amygdule and is no longer restricted to areas adjacent to the fan shaped chlorite aggregates (fc). The development of the (ec) alignment appears best in areas removed from the groundmass (gr), this may be a result of more intense deformation in "unprotected" areas or the size of the fan shaped aggregates was larger nearer the amygdule wall. Bar scale =.25 mm.

A

B

Plate 3

(A) The domainal character of the fabric is clearly visible. Domain 1 (D1) consists of fan shaped chlorite aggregates (fc), oriented at high angles to the Domain 2 (D2) or crenulation cleavage which is characterized by elongate chlorite grains (ec) and actinolite grains (ac) which are aligned parallel to cleavage. Note the cleavage is continuous throughout the plate and shows greater linearity than that shown in plate 2B. Bar scale =.25 mm

(B) This plate is dominated by the the abundance of extremely well oriented elongate chlorite grains (ec) representing the crenulation cleavage. The fan shaped chlorite aggregates (fc) no longer have an arcuate outline, instead , they are appear "rectangular "in shape. Further development of the crenulation cleavage as shown in some high aspect ratio amygdules results in a single domain fabric composed entirely of well oriented elongate chlorite grains. Bar scale== .4 mm.

A

B

illustrate this apparent continuous fabric development. Closer examination of the development of this fabric in the future may prove valuable in our understanding of the evolution of domainal fabric as well as crenulation cleavage.

Correlation between aspect ratio of amygdules and the spacing (as well as the continuity through the amygdule) of the crenulation cleavage. In amygdules of low aspect ratio the crenulation gleavage is widely spaced and irregularly oriented in an arcuate fashion around the fan shaped chlorite aggregates. (Plate 2A). In addition the crenulation cleavage is continuous only over a narrow range ; perhaps one or two fan shaped chlorite aggregates. In amygdules of higher aspect ratio the crenulation cleavage has a much closer spacing and individual cleavages are continuous throughout the entire length of the amygdule. Plates 1 through 3 illustrate this progression.

The relationship between chlorite and epidote grains is complex. In some areas the chlorite wraps around epidote grains (Plate 5). In others the crenulation cleavage has identical orientation on both sides of the epidote grains and appears to "ignore" the presence of the epidote (Plate 5B). Features which are best described as "intermediate" to those outlined above are common. For example, Plate 6A illustrates clearly the "cross-cutting" nature of the crenulation cleavage through the epidote grain, as well as the tendency of the cleavege to "wrap" around the epidote. Another "intermediate " feature is represented in

Plate 4

(A) Differences in fabric development. Fan shaped chlorite aggregates (fc) are found in "protected"areas between epidote (ep) and the groundmass (gr). Elongate chlorite grains (ec) are found in "unprotected " areas generally in the centre of the amygdules. Bar scale = .4 mm.

(B) The appearance of fan shaped chlorite aggregates (fc) near the groundmass (gr) and elongate chlorite (ec) away from the groundmass is common . Bar scale = .25 mm.

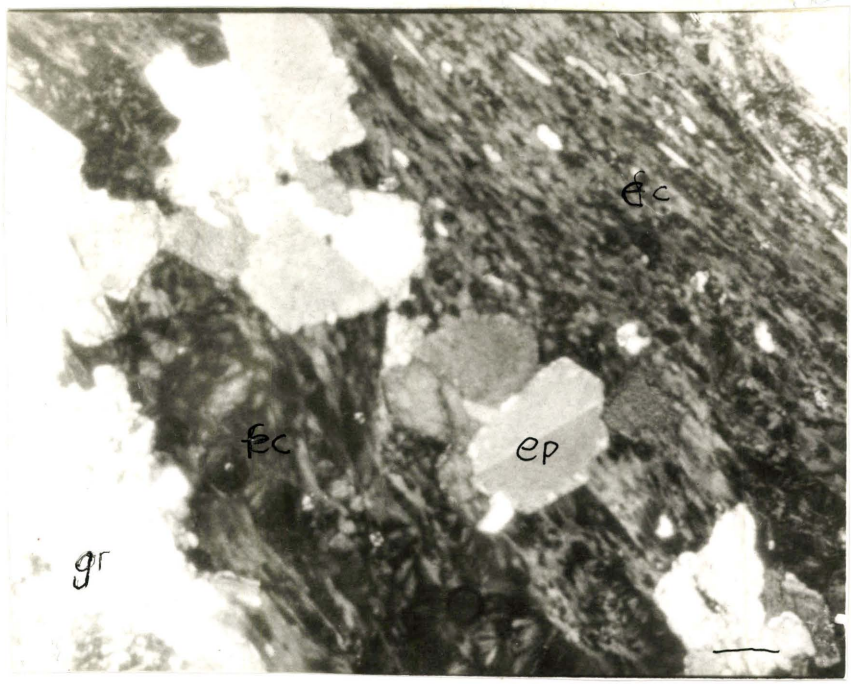

A

B

Plate 5

(A) The "draping" of the crenulation cleavage defined by elongate chlorite (ec) around the epidote grain (ep) is welldefined by the presence of iron oxide staining (io) along the cleavage traces. Randomly oriented chlorite grains are found in the "shadow" produced by the epidote (rc). Bar scale = .4 mm.

(B) The elongate chlorite (ec) appears "ignore" the epidote grain (ep) and immediately adjacent to the epidote it shows no tendency to deflect or change orientation at all. Bar scale = .18 mm.

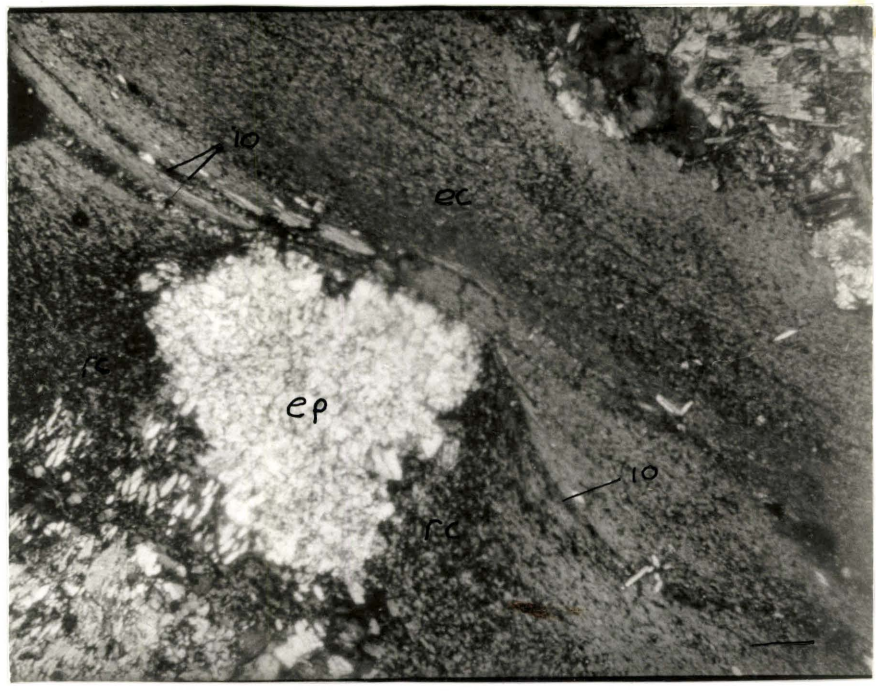

A

B

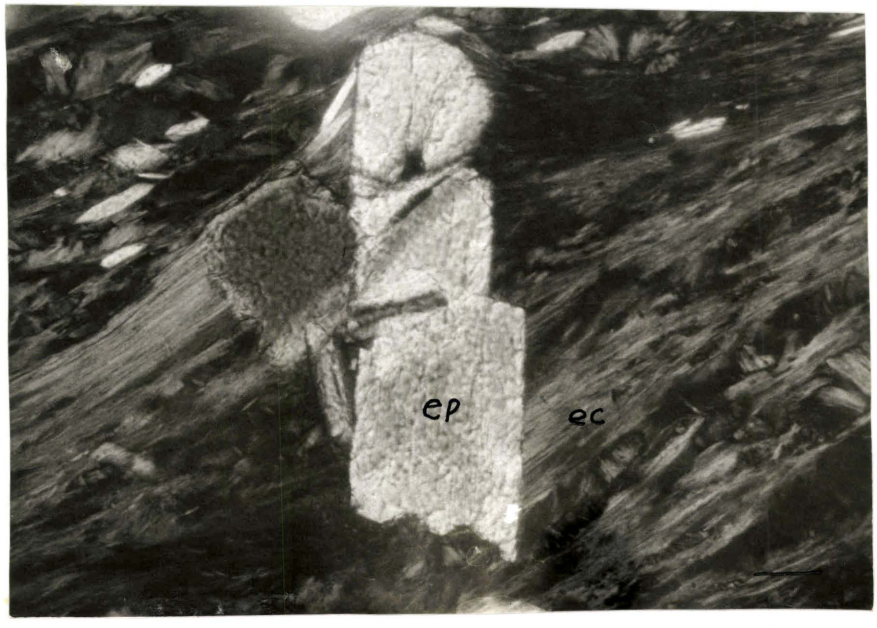

Plate 6B, which clearly shows well defined crenulation cleavage adjacent to an epidote grain (on one side) and a random chlorite fabric on the opposite side. Examination of these relationships leads the author to believe that the epidote crystallized prior to the chlorite and that the chlorite was in a viscous fluid state.

Epidote forms euhedral grains with no evidence of alteration, pressure solution or fracturing. It is commonly situated along the amygdule walls particularly in amygdules possessing high aspect ratios. Although not thoroughly investigated, orientation of the long axes of epidote grains (not in contact with the amygdule wall) appear parallel to the crenulation cleavage and long axis of the amygdule in the XZ plane.

Minor amounts of actinolite in the form of extremely elongate needles penetrate amygdule walls. Isolated needles are only found within the crenulation cleavage and are extremely well oriented and elongate (Plate 7A). Needles which partially penetrate amygdule walls are bent and fractured within the amygdule resulting in parallel orientation to the crenulation cleavage (Plates 8A and 7B). This feature is found in several amygdules and may be useful in determination of the transport direction during the deformation. Small quantities of relict plagioclase grains showing twinning are oriented parallel to the crenulation cleavage where domainal fabric is seen; elsewhere these grains are essentially random in orientation.

Plate 6

(A) Plate illustrating the "dual" nature of the elongate chlorite (ec). The chlorite appears to "drape" around the epidote grain (ep), however at the same time it does seem to cut "through" the epidote and not around it. Bar scale = .4 mm.

(B) Well defined crenulation cleavage (ec) has developed on one side of the epidote grain however the other side is totally unaffected (fc). Bar scale = .18 mm.

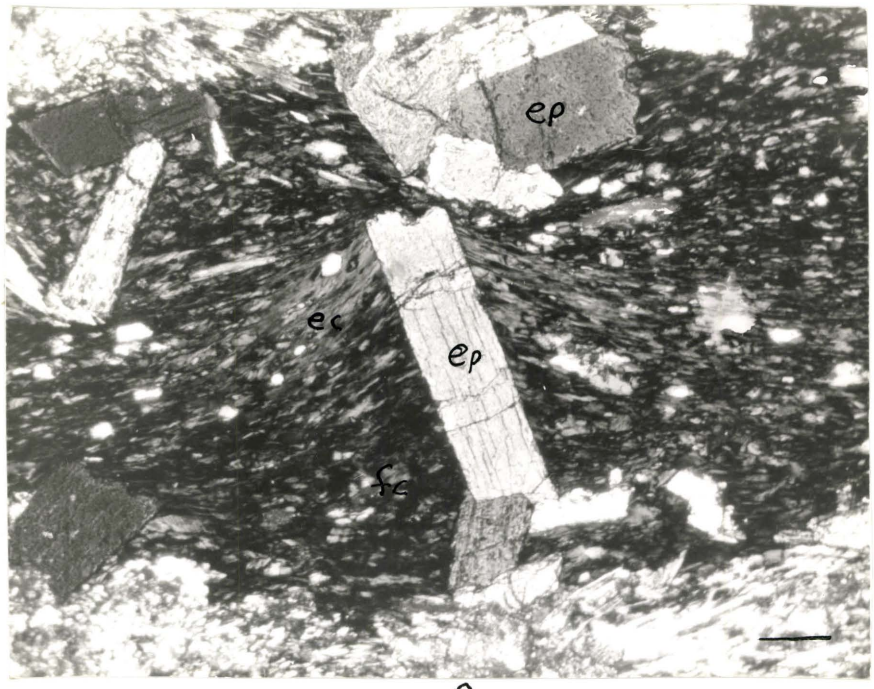

A

B

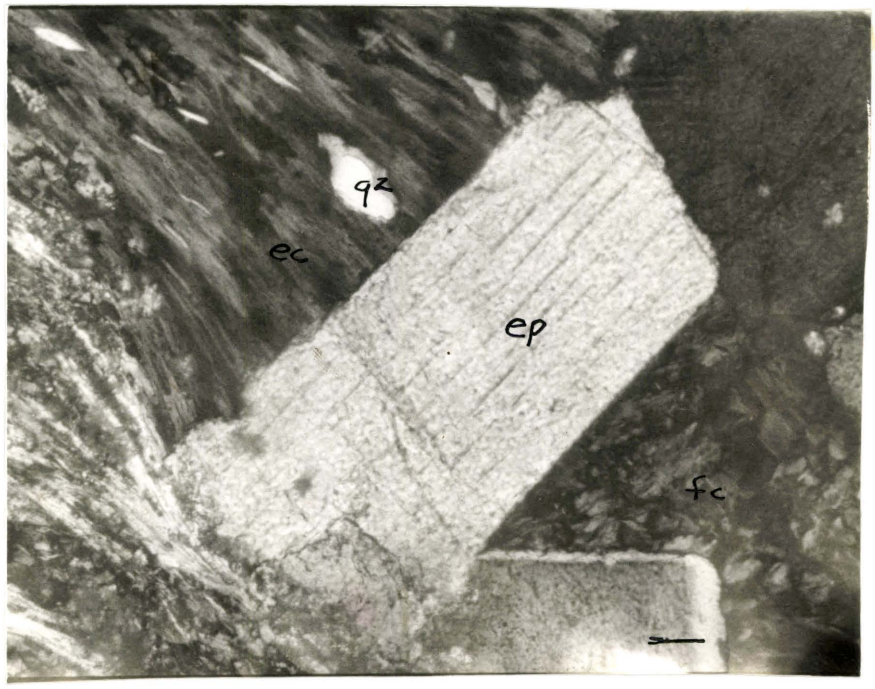

Plate 7

(A) Well oriented elongate actinolite needle (ac) defining the crenulation cleavage. Bar scale = .45 mm.

(B) Change in orientation of actinolite needles (ac) from that in the groundmass (gr) to that in the amygdule (cl). Note the fractures shown by the actinolite within the amygdule. Bar scale = .18 mm.

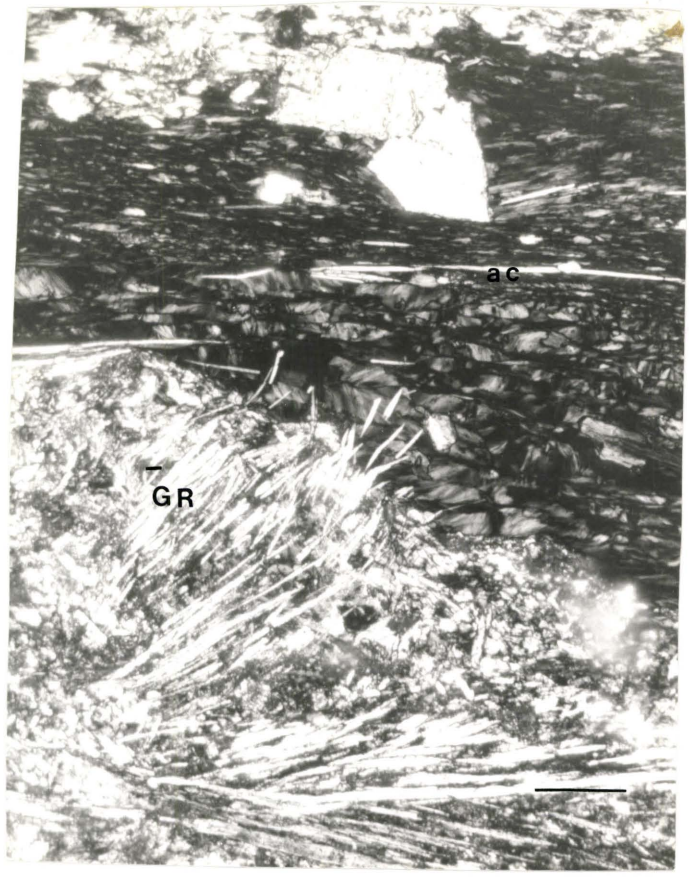

A

B

b) Epidote rich amygdules. These amygdules are generally circular in thin section and contain up 100% epidote. The epidote is distributed evenly throughout the amygdules. Grain shapes are generally subhedral (clearly not as well developed as in the chlorite rich amygdules) and some show distinct parting along cleavage planes. The chlorite occurs as stubby randomly oriented grains which are not as elongate as those found in the chlorite rich amygdules (Plate 8B). Rock cleavage is generally non-existent particularly where chlorite is surrounded by epidote. Domainal fabric is not common. Actinolite needles are not common, however it does penetrate the amygdule where chlorite is adjacent to the wall. The needles are linear and do not appear in an arcuate, fractured, yet continuous state as in chlorite rich amygdules (Plates 7B and 8A). The actinolite is fractured, however it is detached and no longer parallel to that outside the amygdule (Plate 9A). The microstructures found within these amygdules are clearly different from those described in the chlorite rich amygdules. These amygdules appear to have behaved in a rigid manner in contrast to the chlorite rich amygdules.

c) Microstructural relationships between amygdules, groundmass, and cleavage.

Inspection of microstructures within the groundmass indicates the development of similiar domainal fabrics as found in the amygdules. Domain 1 (equivalent to the early schistosity described in the amygdules) is characterized by lath shaped albite,

Plate 8

(A) Change in orientation of an actinolite needle (ac) adjacent to an epidote grain (ep). The actinolite is aligned parallel to the cleavage due to fracturing probably caused by movement of chlorite in the direction of arrow. In order for this to have occurred the epidote grain must have crystalized before the other two minerals. Bar scale = .18 mm.

(B) The random orientation of chlorite grains (sc) within an epidote rich amygdule (ep). Note the short, stubby nature of the grains in contrast to those found in the chlorite rich amygdules. Bar scale = .2 mm.

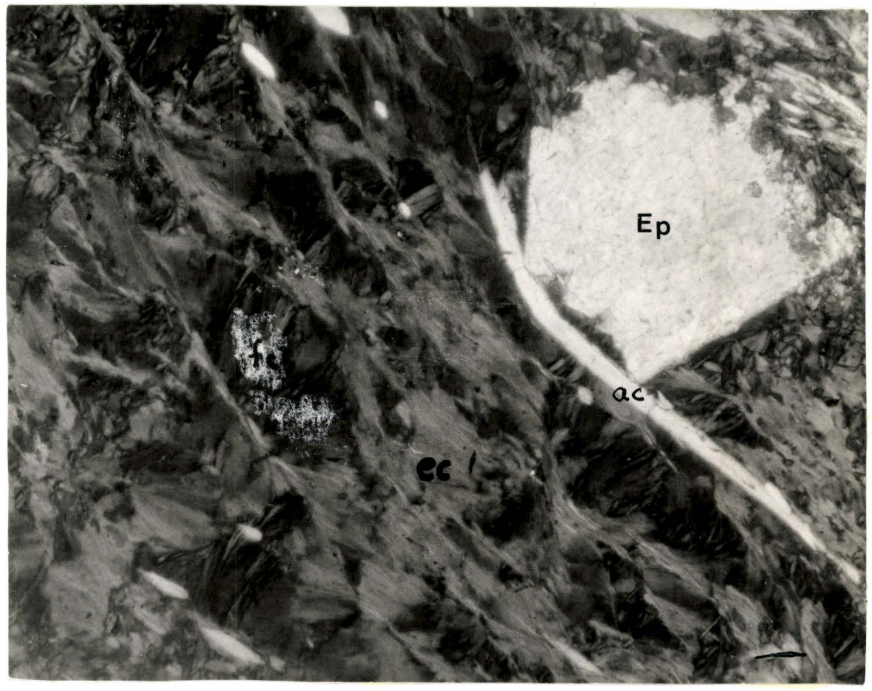

A

B

epidote, interstitial fan shaped chlorite aggregates, actinolite and minor sphene. Domain 2 (equivalent to the crenulation cleavage in the amygdules) consists of elongate actinolite and chlorite grains, and in some areas granulated epidote (Plate 9B). The crenulation cleavage is analogous to the pervasive cleavage in earlier works (Cloos, 1947; Nickelsen, 1956; Reed, 1964). The crenulation cleavage commonly has divergent components which extend around the amygdules as well as a component which penetrates the amygdules. In the lee of the amygdules the three components of cleavage are parallel and equally spaced. The early schistosity consists of rather well oriented albite laths and actinolite needles. These grains are (persistently) found oriented at approximately 60° to the crenulation cleavage (in XZ sections). The albite grains and actinolite needles are commonly fractured either at their extremities or in the middle (or both) creating "V" shaped patterns between the crenulation cleavages (Plate 10A). The remnants of the grains extinguish simultaneously on each side of the medial point of the actinolite needle fractures (Plate 10A). Epidote grains are generally subhedral (rounded) although occasional euhedral grains are encountered. The euhedral grains (particularly longitudinal sections) appear rotated approximately 50-70° relative to the orientation of the crenulation cleavage immediately adjacent to the epidote (Plate 10B). A similiar angular relationship between the rigid epidote rich amygdules and crenulation cleavage is evident. The consistent 50-70° "rotations" are striking.

Plate 9

(A) The deflection of actinolite needles (ac) in an epidote rich amygdule (ep) results in fracture and detachment of needle fragments which remain linear throughout the amygdule and do not show "bending" as those in the chlorite rich amygdules (Plates 7A and 8B). Bar scale = .5 mm.

(B) This plate illustrates the domainal nature of the fabric in the groundmass. The crenulation cleavage is defined by the epidote grains (ep) The early schistosity is characterized by actinolite needles (ac). Bar scale = .2 mm.

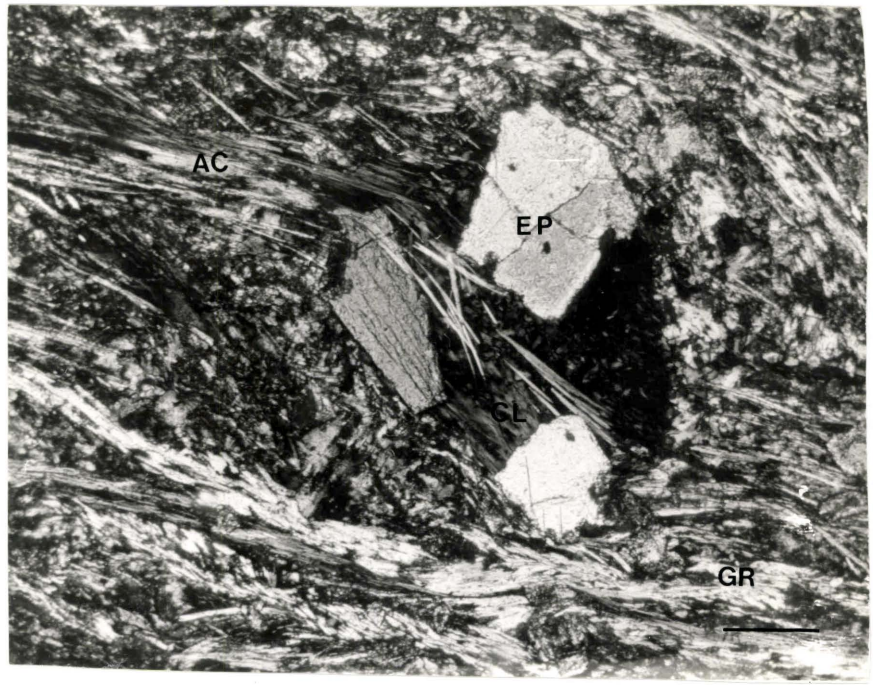

A

B

CHAPTER IV

STRUCTURAL IMPLICATIONS OF MICROSTRUCTURES AND STRUCTURAL ANALYSIS

1. NATURE AND GENERATION OF THE EARLY SCHISTOSITY AND THE CRENULATION CLEAVAGE

The formation of cleavage appears to involve a variety of mechanisms. Evidence of mechanical rotation, mechanical flattening, recrystallization, growth of new minerals with preferred orientation, and flattening are seen. Evidence for mechanical rotation have been discussed previously. The rotation is shown by variable orientation of actinolite needles in epidote and plagioclase grains as well as in epidote rich amygdules (Plates 10B and 11A). Evidence of mechanical flattening includes granulation and orientation of epidote parallel to the crenulation cleavage and the flattening of amygdules (from the deformation path). Recrystallization and growth of new minerals with preferred orientation is shown primarily by actinolite and chlorite grains. The needles (actinolite and chlorite) within the crenulation cleavage are consistently longer than those in the early schistosity and are extremely well oriented.

Plate 10

(A) The "V" shaped pattern produced in actinolite needles (ac) defining the early schistosity is evident due to the extinguished fragments to the right. The early shistosity is bounded by granulated epidote grains (ep) defining the crenulation cleavage. Note that the actinolite needles are inclined at approximately 60° to the cleavage. Bar scale = .18 mm.

(B) The epidote grain (ep) appears to have undergone a rotation as marked by the arrows. Bar scale = .5 mm.

A

B

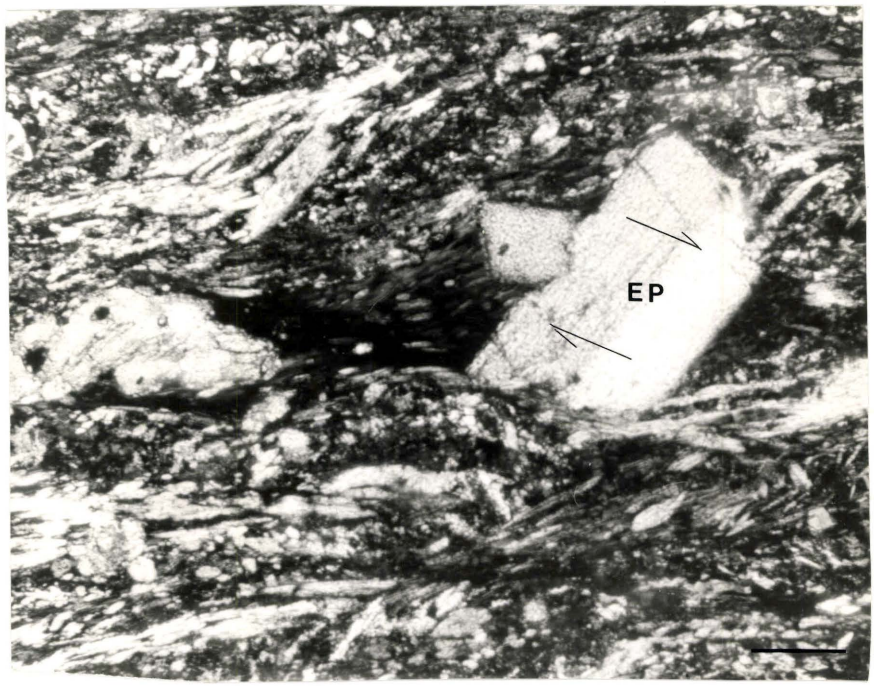

Plate 11

(A) The relict plagioclase grain appears to have undergone a rotation as marked by the arrows. Bar scale = .5 mm.

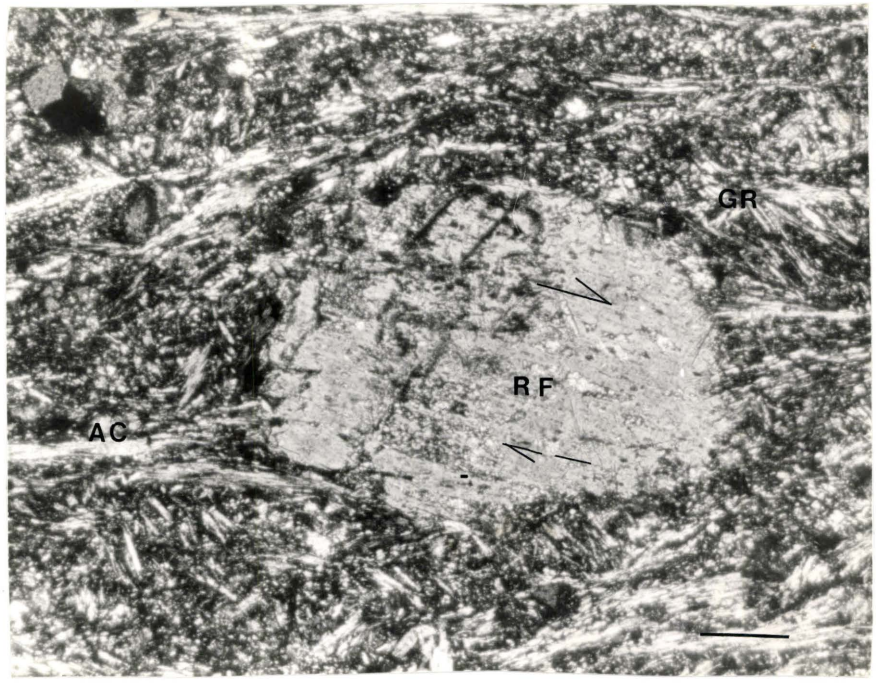

A

Although cleavage formation is a result of a variety of mechanisms, individual mechanisms may be important at certain stages of the deformation. Ramsay (1967) has suggested that mechanical rotation may be a most important process at lowest metamorphic grades, with recrystallization being of greatest importance under high temperature conditions. The metabasalts of greenschist facies occupy an intermediate position within the continuum of these processes and both kinds of features are common.

Whether the cleavage is a flattening or shearing phenomenon is difficult to ascertain. Evidence for a shearing origin appear to be most satisfactory for the following reasons.

i) The cleavage (crenulation) only appears obvious in "unprotected"(epidote poor) areas in the chlorite rich amygdules and appears to "flow" around epidote grains, whereas in "protected" (epidote rich) areas no such pattern is obvious (Plates 4A and 6A).

ii) The solid-body rotations exhibited by plagioclase, epidote, and rigid epidote rich amygdules with no evidence of pressure solution is more probable in a shearing process.

iii) The apparent movement of material suggested by actinolite needles protruding through amygdule walls and their fracture patterns is highly improbable in a true flattening concept of cleavage formation.

There is evidence however that the initial early schistosity may have been produced during an episode of flattening. The evidence includes:

i) The results obtained from the structural analysis of amygdules indicates an initial flattening episode.

ii) The appearance of parallel apparently unsheared chlorite in areas protected by epidote grains may have resulted from an initial flattening episode.

iii) The consistent alignment of relict feldspar laths as well as actinolite needles at high angles (50- 70°) to the crenulation cleavage may well represent rotation of laths due to flattening to form the initial early schistosity.

From this previous discussion the author suggests that an original crude schistosity developed perpendicular to the direction of maximum finite shortening due to stress exerted by overlying rock (particularly during the early phase of metamorphism). Subsequently, forces induced motions in a westerly and upward direction, creating a crenulation cleavage inclined at relatively high angles to the early schistosity. This proposal would imply that the orientation of the original flow top would be equivalent to the orientation of grains of the early schistosity (provided these are still unrotated).

In summary the cleavages appear to be formed by a complex

interplay of several mechanisms. The early schistosity may have been formed at lower temperatures primarily by mechanical rotations, produced by flattening as a result of stresses exerted by overlying rock strata. The crenulation cleavage is a higher temperature phenomenon with recrystallization of oriented minerals being the single most important formation mechanism.

2. PRESENCE OF CRENULATION CLEAVAGE IN A METABASALT

No record of a crenulation cleavage within a metabasalt was encountered in the literature cited. This is not surprising since one would not expect to find such a feature in a basalt which originally possessed a random fabric. Crenulation cleavage tends to develop in rocks which exhibit well developed mineral orientation (schistosity)(Gray, 1978). Although the original fabric is not conducive to crenulation cleavage formation, the grade of metamorphism (greenschist) certainly is , as most crenulation cleavage is of this facies (Gray,1977). There is no valid reason to suspect that crenulation cleavage could not be developed in metabasalts, particularly those which have undergone an initial flattening episode. This flattening creates an early schistosity, probably similiar, though not as well defined as in well layered sedimentary rocks. Thus the basalt requires an initial flattening episode followed by a deformation to form

the crenulation cleavage , whereas the sedimentary rock merely requires one deformation event. The relatively poor crenulation cleavage development (in contrast to some metasediments) is likely due to the "crude" orientation of the early schistosity.

3. TECTONIC TRANSPORT DIRECTION

The orientation and to a lesser extent the nature of material movement can be established from previous analyses. The deformation indicates that the amygdules were initially flattened and subsequently deformed according to a plane strain mechanism. Presumably tectonic transport took place with the same orientation as the X principal strain axis for the tectonic strain ellipsoid. This would be in an orientation of 127/57° E or along planes oriented at 037/57°E.

Close examination of microstructures; specifically;

i) the sense of rotation established for rigid epidote rich amygdules, epidote grains, and relict feldspars within the groundmass,

ii) the fracture patterns (V-shaped) produced by actinolite needles in the early schistosity between the crenulation cleavage,

and iii) the arcuate, fractured actinolite needles partially intruding the amygdule walls, all indicate the

movement of material was "updip" in a westerly direction. This agrees with Cloos (1948); he states: "with few exceptions the lineation has an azimuth of 120- 130° and plunges of 10 - 50° east",(Cloos,1958,pg.66) also "there seems little doubt that the Blue Ridge crystallines have moved considerable distances westward, and upward"(Cloos,1971, pg.113).

4. PROPOSED SEQUENCE OF STRUCTURE DEVELOPMENT

The examination of microstructures as well as the structural analysis of amygdule shapes, allows one to postulate a sequence of events leading to the present features observed. The sequence is discussed below and is illustrated in figure 25.

i) The emplacement of subaerial tholeiitic basalt flows consisting of initially sub-spherical to spherical amygdules enclosed by a randomly oriented fabric composed of feldspar laths, pyroxenes, interstitial chloritic material and isolated porphyritic feldspar laths.

ii) This is followed by slight compression due to accumulation of overlying sediment. This may be accompanied by zeolite growth in the amygdules and fracturing of the basalt with subsequent introduction of epidote and quartz into these fractures.

iii) In the early stages of metamorphism (moderately low temperatures) epidote forms within the amygdules as well as

Figure 25. Proposed Sequence of Structure Development

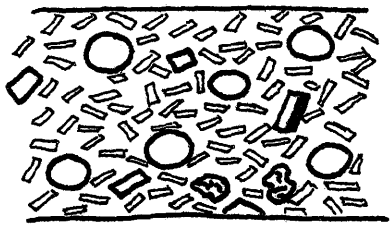

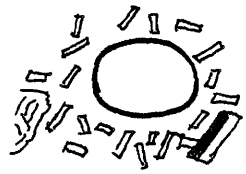

i) Emplacement of Basalt

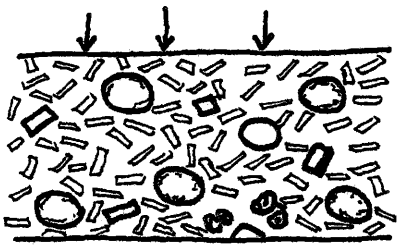

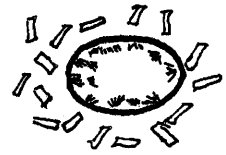

ii) Slight Compression due to overlying strata

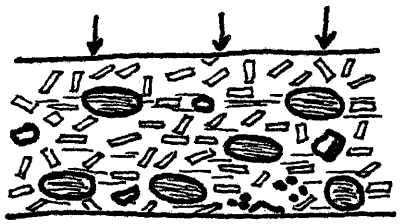

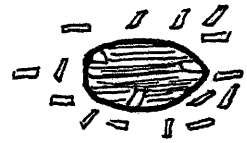

iii) Compression in early stage of deformation forming schistosity

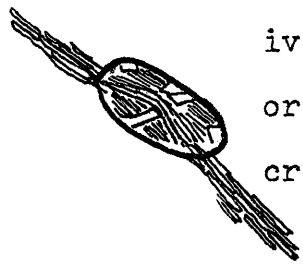

iv) Change in stress orientation creates the crenulation cleavage

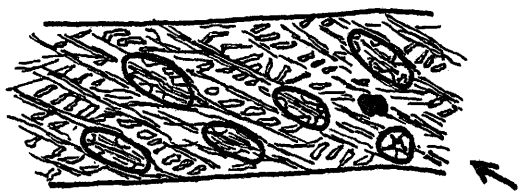

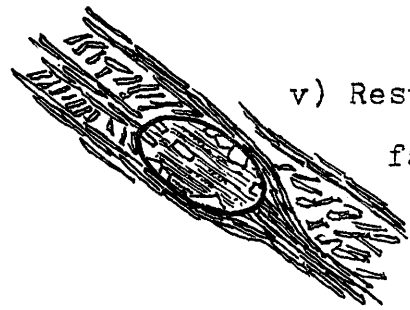

v) Resultant domainal fabric.

in the groundmass as a replacement of pyroxene. Segregation of epidote and chlorite rich amygdules probably occurs at this stage. Segregated epidote and quartz fill in former fractures and cavities forming epidosite bodies. Mechanical rotation caused by compression results in a crude early schistosity oriented perpendicular to the compression direction. Migration of chloritic material into amygdules commenced resulting in alignment of chlorite (long axes) perpendicular to the stress direction. In the groundmass epidote and actinolite replace pyroxene grains and chlorite replaces plagioclase.

iv) During the peak stages of metamorphism material is transported westward along recently formed cleavage planes oriented approximately 60° to the early schistosity, occurs. Elongation of chlorite rich amygdules and rotation of epidote rich amygdules, epidote, and relict feldspars proceeds. Actinolite and chlorite needles crystallize in a well oriented fashion forming the crenulation cleavage. Occasional actinolite needles penetrating amygdule walls are fractured and deflected due to motion of chlorite within the amygdules. The "V"- shaped pattern produced by the fractured actinolite in the early schistosity appears to be a result of rotation of needles which are longer than the spacing of the crenulation cleavage. Therefore further rotation is not possible without fracturing, which result in the "V"- shaped pattern.

v) The end of metamorphism is marked by continued actinolite and chlorite growth accentuating the crenulation cleavage.

CHAPTER V

CONCLUSION

The Catoctin Formation east of Cavetown, Maryland in the overturned limb of the South Mountain Anticline is a greenschist grade metabasalt characterized by the albite-chlorite-actinolite-epidote mineral assemblage. Intense shearing has obliterated the original igneous textures, but elsewhere, relict basaltic texture is known (Reed, 1964).

A consistent lineation comprised of well oriented ellipsoidal chlorite amygdules is found within Catoctin Volcanic flow tops. The orientation of the lineation was determined to be $127/57^{\circ}$ E using fluctuation plot data. Rapid inspection of the amygdules in the field would undoubtedly be a simpler, faster method of estimating this, with comparable results.

Studies from recent tholeiitic basalt flows indicate amygdules within flow tops are nearly spherical. Computation of the original shapes of amygdules using methods proposed by Ramsay(1967), Hsu (1970), and Wood (1974) indicate original non-spherical shapes. This suggests that the amygdules may have been flattened prior to the development of the crenulation cleavage.

Determination of the tectonic strain ellipsoid using methods outlined by Ramsay (1967) and Hsu (1970) produce comparable

results. The orientation of the principal axes of the tectonic strain ellipsoid are shown in Figure 21.

The construction of a deformation path similiar to that of Wood (1974) is a useful concept, however the graphical representation of the deformation path is much easier to interpret using a logarithmic scale than the arithmetic scale employed by Wood. Both the logarithmic plot (described above) and the Flinn plot clearly indicate an initial flattening episode followed by approximately plane strain.

Examination of microstructures (in both amygdules and groundmass) reveals a distinct domainal fabric consisting of an early schistosity and a crenulation cleavage. This domainal character is not found within epidote rich amygdules. There appears to be definite correlations between the XZ aspect ratios of chlorite rich amygdules on the one hand, and spacing, continuity and linearity of the crenulation cleavage within the amygdules on the other. In a broad sense comparison of progressively higher aspect ratios (of amygdules) parallels the origin, development, and destruction of the domainal fabric. Therefore careful examination of a few well chosen amygdules may yield information concerning the evolution of both domainal fabric and crenulation cleavage.

BIBLIOGRAPHY

AUMENTO, F., 1971, Vesicularity of mid-oceanic pillow lavas: Canadian Jour. of Sciences., v. 8, p. 1315-1319

BASCOM, F., 1893, Structures, origin and nomenclature of the acid volcanic rocks of South Mountain: Jour. of Geol., v.1, p. 813-832.

BLOOMER, R.O., and WERNER, H.J., 1955, Geology of the Blue Ridge Region in central Virginia: Geol. Soc. of America Bull., v.66, p. 579-606.

CLOOS, ERNST, 1971, Microtectonics along the western edge of the Blue Ridge, Maryland and Virginia: John Hopkins Press, Baltimore and London.

_____, 1958, Guidebooks 4&5, Structural geology of South Mountain and Appalachians in Maryland: John Hopkins Univ. Studies in Geology, Pettijohn, F.J., ed., John Hopkins Press.

DUNNET, D., 1969, A technique of finite strain analysis using elliptical particles: Tectonophysics, v.7, p. 117-136.

DURNEY, D.W., 1972, Solution transfer, an important geological deformation mechanism: Nature, v.235, p. 315-317.

ESPENSHADE, GILBERT H., 1970, Geology of the northern part of the Blue Ridge anticlinorium, in Fisher, G.W. et al., eds., Studies of Appalachian geology: Interscience Publ., New York.

GROSHONG, H., 1976, Strain and pressure solution in the Martinsburg slate Delaware water gap, New Jersey: American Jour. Sci., v.276, p. 1131-1146.

GAY, N. C., 1968, Pure shear and simple shear deformation of inhomogeneous viscous fluids. 2. The determination of the total finite strain ina rock from objects such as deformed pebbles: Tectonophysics, v.5(4), p. 295-302.

GRAY, D.R., 1978, Cleavages in deformed psammitic rocks from southeastern Australia; Their nature and origin: Geol. Soc. of America Bull., v.89, p. 577-590.

———, 1977, Some parameters which affect the morphology of crenulation cleavages: Jour. of Geol., v.85, p. 763-780.

____, 1979, Microstructure of crenulation cleavages; an indicator of cleavage origin: American Jour. of Sci. v.279, p. 97-128.

HIGGINS, MICHEAL W., 1971, Depth of emplacement of James Run Formation pillow basalts, and the depth of deposition of part of the Wissahickon Formation, Appalachian Piedmont, Maryland: American Jour. of Sci., v.271, p. 321-332.

HOBBS, BRUCE E., MEAN, WINTHROP D., and WILLIAMS, PAUL F., 1976, An outline of structural geology: John Wiley and Sons, Inc., New York, 571 p.

HOSSACK, J.R., 1968, Pebble deformation and thrusting in the Bygdin area (Southern Norway): Tectonophysics, v.5(4), p. 315-339.

HSU, MAO-YANG, 1971, Analysis of strain, shape and orientation of the deformed pebbles in the Seine River area, Ontario: PHD thesis, McMaster University, Hamilton, Ontario.

JOLLY, WAYNE T.,and SMITH, RAYMOND E., 1972, Degradation and metamorphic differentiation of the Keweenawan tholeitic lavas of Northern Michigan, U.S.A.: Jour. of Petrology, v.13,part 2, p. 273-309.

KERR, PAUL F., 1959., Optical Mineralogy, 3rd edition, McGraw-Hill Book Co. Inc.

MITRA, SHANKAR, 1978, Microscopic deformation mechanisms and flow laws in quartzites within the South Mountain anticline: Jour. of Geol., v.86, p. 129-152.

NICOLAS, A., and POIRIER, J.P., 1976, Crystalline plasticity and solid state flow in metamorphic rocks, John Wiley & Sons, Ltd., London.

NICKELSEN, RICHARD P., 1956, Geology of the Blue Ridge near Harper's Ferry, West Virginia: Geol. Soc. Amer. Bull., v.67, p. 239-270.

RAMSAY, JOHN G., and WOOD, DENNIS S., 1973, The Geometril effects of volume change during deformation processes: Tectonophysics, v.16, p. 263-278.

____, 1976, Displacement and strain: Phil Trans. Roval Soc., London, A. v.283, p. 3-25.

RAMSAY, JOHN G., 1963, Structural investigations in the Barberton Mountain Land, Eastern Transvaal., Trans. Geol Soc. S. Africa, v.66, p. 353-401.

____, 1967, Folding and fracturing of rocks, Mcgraw-Hill, New York, 568p.

REED, JOHN C. JR., 1964, Chemistry of greenstone of the Catoctin Formation in the Blue Ridge of Central Virginia: U.S. Geol. Survey Prof. Paper, No.501C, p. C69-C73.

____, and BENJAMIN, A.M., 1971, Chemical alteration and splitization of the Catoctin greenstones, Shenandoah National Park, Virginia: Jour. of Geol., v.69, p.526-548.

____, 1955, Catocin formation near Luray, Virginia: Geol. Soc. of Amer. Bull., v.66. p. 871-896.

ROY, ASHIT BARAN, 1978, Evolution of slaty cleavage in relation to diagenisis and metamorphism: A study from the Hunsruckschiefer: Geol. Soc. of Amer. Bull., v.89, p. 1775-1785.

STAUFFER, R., 1970, Deformation textures in tectonites: Canadian Jour. of Earth Sciences, v.7, p. 499-511.

VALLANCE, T.G., 1974, Spilitic degradation of a tholeitic basalt: Jour. of Petrology, v.15, part 1, p. 79-96.

WHITAKER, J.C., 1955, Geology of Catoctin Mountain: Geol. Soc. of Amer. Bull., v.66, p. 435-462.

WILLIAMS, P.F., 1972, Development of metamorphic layering and cleavage in low grade metamorphic rocks at Bermagui, Australia: Amer. Jour. of Sci., v.272, p. 1-47.

WOOD, DENNIS S., 1974, Current views of the development of slaty cleavage: Annual Review of Earth and Planetary Sciences, v.2, p. 369-400.

____, 1973, Patterns and magnitudes of natural strain in rocks: Phil. Trans. Royal Soc. London, A, v.274, p. 373-382.

APPENDIX

A. Methods and Procedures

Measurements were made on the chlorite amygdules found within the Catoctin Volcanics in the study area just east of Cavetown, Maryland. The basic procedure is outlined below:

i) The attitude of the cleavage plane was recorded and labelled on the rock specimens in the field.

ii) The samples were removed and taken to the laboratory where the best approximation to the principal ellipsoid axes were marked.

iii) Two specimens were cut in the XY, ZY, and XZ orientation of the ellipsoids (approximate)(see Figure 26).

iv) Thin sections were obtained for each plane of both specimens.

v) The thin sections were studied structurally as well as petrographically.

vi) Re-orientation of data with that obtained in the field was completed.

vii) All data was plotted onto graphs, diagrams and tables.

Cutting of specimens along the principal axes of the amygdules was purely subjective and undoubtedly a small error is produced. Approximately 40-50 amygdules were mesured for each plane. Chlorite rich amygdules were treated independently from the epidote rich variety.

Figure 26. Procedure of Slabbing:
Planes produced by slabbing specimens.

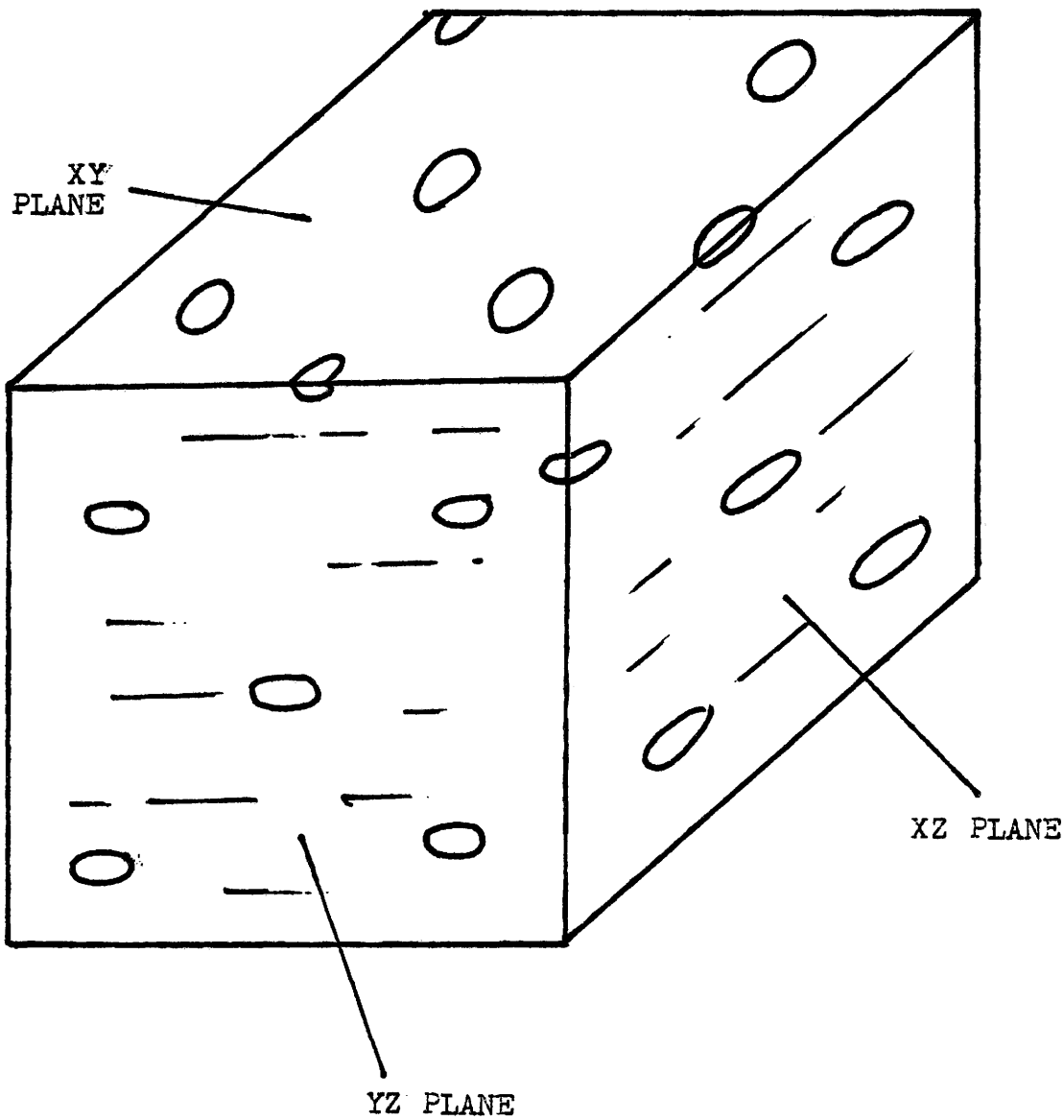

APPENDIX B — RAW DATA

XY PLANE SPECIMEN 1

LONG AXIS (X) (mm.)	SHORT AXIS (Y) (mm.)	(Ø)	X/Y	LOG X/Y	X/Y
4.2	2.1	10	2.0	.30	1.41
.75	.5	12	1.5	.18	1.22
1.0	.8	18	1.25	.096	1.12
1.5	1.2	30	1.25	.096	1.12
1.7	.9	22	1.8	.256	1.34
2.0	1.4	10	1.42	.15	1.19
* .7	.6	65	1.17	.07	1.08
2.6	1.25	8	2.11	.324	1.45
4.8	2.4	14	2.0	.30	1.41
1.0	.7	32	1.4	.146	1.2
*1.3	1.2	65	1.1	.414	1.05
*1.1	1.0	58	1.1	.414	1.05
2.2	1.35	9	1.57	.196	1.3
2.3	1.6	38	1.4	.196	1.2
1.1	.8	30	1.38	.14	1.17
.9	.7	25	1.29	.11	1.14
*1.1	1.0	53	1.10	.41	1.05
* .8	.7	54	1.17	.068	1.08
1.0	.7	15	1.43	.156	1.2
2.4	1.5	24	1.6	.20	1.26
3.0	1.8	25	1.67	.222	1.3
3.7	2.5	22	1.48	.17	1.22
4.6	3.0	15	1.23	.089	1.11
2.7	2.2	40	1.29	.089	1.14
2.5	2.1	0	1.19	.076	1.09
4.0	2.7	3	1.48	.17	1.22

* indicates epidote rich amygdule

LONG AXIS (X) (mm.)	SHORT AXIS (Y) (mm.)	(Ø)	X/Y	LOG X/Y	$(X/Y)^{\frac{1}{2}}$
1.8	.9	3	2.0	.30	1.41
2.0	1.5	28	1.33	.125	1.15
*2.8	1.5	60	1.2	.08	1.1
*1.4	1.2	70	1.17	.067	1.08
*1.0	.9	72	1.1	.045	1.05
63.95	42.7		44.2		36.9 TOTALS

YZ PLANE SPECIMEN 1

LONG AXIS (Y) (mm.)	SHORT AXIS (Z) (mm.)	(Ø)	RATIO (Y/Z)	RATIO (Z/Y)	LOG (Z/Y)
1.8	.65	4	2.9	.36	-.44
1.9	1.1	7	1.7	.59	-.23
1.1	.7	4	1.6	.63	-.20
1.0	.7	0	1.4	.71	-.15
1.1	.4	12	2.7	.37	-.43
1.5	.7	8	2.1	.48	-.32
1.2	.7	9	1.7	.59	-.23
1.5	.6	3	2.5	.4	-.40
2.8	1.3	24	2.2	.45	-.34
2.2	1.1	19	2.0	.5	-.30
1.9	.7	11	2.7	.37	-.43
1.8	.7	11	2.6	.38	-.41
1.0	.9	12	1.1	.91	0.04
1.4	.9	10	1.6	.63	-.20
2.1	.7	12	3.0	.33	-.48
2.5	1.2	17	2.1	.48	-.32
1.8	.7	7	2.1	.48	-.32
.9	.5	2	1.8	.55	-.26
2.0	.7	11	2.9	.34	-.46
1.8	.9	9.	2.0	.5	-.30
* .9	.85	70	1.1	.91	-.04
1.1	.5	13	2.2	.45	-.34
1.3	.7	11	1.9	.53	-.28
1.0	.6	5	1.7	.59	-.23
1.4	.6	1	2.3	.43	-.36

LONG AXIS (Y) (mm.)	SHORT AXIS (Z) (mm.)	(Ø)	RATIO (Y/Z)	RATIO (Z/Y)	LOG (Z/Y)
1.2	.6	8	2.0	.5	-.30
1.0	.8	12	1.3	.77	-.11
*1.0	.9	62	1.1	.91	-.04
*1.4	1.2	40	1.15	.87	-.61
2.1	1.1	11	1.9	.53	-.28
2.2	1.3	17	1.7	.59	-.23
1.4	.5	20	2.9	.39	-.46
1.6	.9	16	1.78	.56	-.25
.8	.6	21	1.3	.77	-.11
1.0	.8	20	1.3	.77	-.11
1.4	1.2	21	1.2	.83	-.08
1.4	.8	9	1.8	.56	-.36
1.1	.7	9	1.6	.63	-.20
1.4	.7	6	2.0	.5	-.30
1.2	.5	7	2.4	.42	-.38
* .6	.55	71	1.02	.98	-.09
1.5	.7	16	2.14	.47	-.33
1.8	1.5	0	1.2	.83	-.08
2.0	1.1	12	1.82	.55	-.26
2.4	1.6	12	1.5	.67	-.18
. 2.0	1.8	75	1.1	.9	-.05
1.4	1.3	66	1.08	.93	-.03
2.7	1.2	5	2.25	.44	-.35
1.5	1.5	-	1.0	1.0	-.00
1.6	1.4	70	1.14	.88	-.058
.9	.8	50	1.13	.89	-.05
74.0	44.6		92.6	31.1	TOTALS

XZ PLANE SPECIMEN 1

LONG AXIS (X) (mm.)	SHORT AXIS (Z) (mm.)	(Ø)	X/Z	$(X/Z)^{\frac{1}{2}}$
1.5	.5	12	3.0	1.732
1.7	.3	17	5.7	2.39
3.1	1.1	2.0	2.82	1.68
1.3	.5	11	2.6	1.6
1.35	.75	11	1.8	1.34
1.5	.8	10	1.88	1.37
1.4	.8	16	1.75	1.32
2.1	1.1	12	1.91	1.38
1.7	.8	15	2.13	1.46
2.35	1.2	8	2.0	1.41
3.3	.9	12	3.67	1.92
4.0	1.2	10	3.33	1.82
1.9	1.0	11	1.9	1.38
2.4	.8	10	3.0	1.73
1.2	.6	8	2.0	1.41
2.4	1.0	8	2.4	1.55
4.4	1.2	14	3.67	1.92
1.5	.7	8	2.14	1.46
2.1	.7	0	3.0	1.73
2.5	.9	14	2.78	1.67
2.7	1.2	14	2.25	1.5
1.4	.5	6	2.8	1.67
1.8	.8	9	2.25	1.5
1.8	.8	8	2.25	1.5
.8	.6	15	1.33	1.15

LONG AXIS (X) (mm.)	SHORT AXIS (Z) (mm.)	(ø)	X/Z	$(X/Z)^{\frac{1}{2}}$
2.0	.8	17	2.5	1.58
2.0	.7	17	2.86	1.36
4.4	1.2	10	3.67	1.92
.8	.6	3	1.33	1.15
1.2	.3	20	4.0	2.0
1.2	.3	2	4.0	2.0
4.3	1.3	13	3.3	1.82
3.9	1.0	8	3.9	1.98
1.8	1.0	18	1.8	1.34
1.4	.7	10	2.0	1.41
.9	.3	17	3.0	1.73
1.1	.6	14	1.83	1.35
3.4	1.0	8	3.4	1.84
.9	.5	10	1.8	1.34
1.6	.4	12	4.0	2.0
2.4	.6	13	4.0	2.0
.7	.5	9	1.4	1.2
3.0	1.0	12	3.0	1.73
4.0	.9	11	4.4	2.1
5.2	.8	10	6.5	2.55
3.2	.7	11	4.6	2.14
2.8	1.0	11	2.8	1.67
3.5	.6	12	5.8	2.41
3.5	2.0	9	1.8	1.34
4.2	.7	11	6.0	2.5

LONG AXIS (X) (mm.)	SHORT AXIS (Z) (mm.)	(ø)	X/Z	$(X/Z)^{\frac{1}{2}}$	
*1.2	1.1	74	1.1	1.05	
2.0	1.0	12	2.0	1.41	
5.0	1.0	8	5.0	2.22	
*1.5	1.3	70	1.2	1.1	
121.6	43.7		157.3	89.8	TOTALS

XY PLANE SPECIMEN 2

LONG AXIS (X) (mm.)	SHORT AXIS (Y) (mm.)	(Ø)	X/Y	LOG X/Y	$(X/Y)^{\frac{1}{2}}$
2.0	1.3	15	1.54	.19	1.24
6.0	4.5	15	1.33	.12	1.15
5.0	3.0	20	1.67	.22	1.29
5.5	4.0	13	1.38	.14	1.17
2.0	1.5	14	1.38	.12	1.15
3.3	2.0	19	1.65	.22	1.28
4.0	2.0	15	2.0	.30	1.41
4.6	3.2	18	1.44	.16	1.2
5.0	3.0	22	1.67	.22	1.29
9.0	6.0	18	1.5	.18	1.2
2.0	1.2	16	1.67	.22	1.29
3.0	2.0	16	1.5	.18	1.2
2.0	1.2	15	1.67	.22	1.29
4.7	3.0	15	1.57	.19	1.25
3.0	1.9	19	1.56	.19	1.25
7.0	4.5	14	1.56	.19	1.25
5.0	3.0	27	1.67	.22	1.29
4.3	3.5	28	1.23	.09	1.11
5.0	3.5	18	1.43	.16	1.2
*3.5	3.3	27	1.06	.03	1.03
*4.0	3.8	80	1.05	.03	1.02
1.8	1.5	18	1.2	.08	1.1
2.7	1.0	18	2.7	.43	1.64
2.0	1.4	21	1.43	.16	1.2
3.0	2.1	16	1.43	.16	1.2

LONG AXIS (X) (mm.)	SHORT AXIS (Y) (mm.)	(Ø)	X/Y	LOG X/Y	X/Y	
*2.8	2.5	70	1.12	.05	1.06	
2.0	1.1	14	1.82	.26	1.35	
2.2	1.9	34	1.16	.06	1.08	
7.0	4.0	19	1.75	.24	1.32	
*5.5	5.0	71	1.1	.04	1.05	
5.0	3.2	17	1.56	.19	1.25	
*3.0	2.7	69	1.11	.04	1.05	
3.0	2.4	20	1.25	.097	1.12	
5.0	3.1	21	1.61	.21	1.27	
5.0	3.0	13	1.66	.22	1.28	
4.0	2.1	11	1.9	.28	1.4	
143.9	98.4		55.9		46.2	TOTALS

YZ PLANE SPECIMEN 2

LONG AXIS (Y) (mm.)	SHORT AXIS (Z) (mm.)	(Ø)	Y/Z	Z/Y	LOGY/Z	$(Y/Z)^{\frac{1}{2}}$
4.0	2.0	20	2.0	.5	-.30	1.41
5.0	2.0	15	2.5	.4	-.40	1.58
3.0	1.5	14	2.0	.5	-.30	1.41
2.0	1.5	19	1.33	.72	-.92	1.15
4.0	1.2	14	3.3	.30	-.52	1.82
5.0	2.0	11	2.5	.4	-.90	1.58
4.0	1.0	14	4.0	.25	-.60	2.0
4.0	1.0	12	4.0	.25	-.60	2.0
1.5	.7	14	2.1	.48	-.32	1.42
4.0	3.0	9	1.33	.75	-.12	1.15
3.0	1.0	14	3.0	.33	-.47	1.73
4.0	3.0	12	1.33	.74	-.12	1.15
5.0	2.5	8	2.0	.51	-.3	2.0
4.0	2.5	10	1.6	.63	-.20	1.27
6.0	3.0	11	2.0	.5	-.30	1.41
2.5	1.5	9	1.4	.71	-.15	1.2
2.0	.75	8	2.7	.37	-.43	1.64
4.0	2.5	11	1.6	.63	-.20	1.27
4.0	2.0	12	2.0	.52	-.30	1.41
*5.0	4.3	52	1.1	.91	-.04	1.05
3.5	1.0	7	3.5	.29	-.54	1.87
3.0	2.0	9	1.66	.60	-.22	1.29
3.0	1.0	8	3.0	.33	-.47	1.72
3.5	1.5	3	2.33	.43	-.37	1.53
4.0	2.5	20	1.33	.74	-.12	1.15

LONG AXIS (Y) (mm.)	SHORT AXIS (Z) (mm.)	(ø)	Y/Z	Z/Y	LOGY/Z	Y/Z	
2.0	1.0	9	2.0	.51	-.30	1.41	
4.0	1.7	10	2.38	.42	-.38	1.54	
3.5	3.0	11	1.17	.85	-.07	1.08	
4.0	2.0	13	2.0	.5	-.30	1.41	
5.0	4.0	16	1.25	.8	-.10	1.12	
5.0	2.5	14	2.0	.51	-.30	1.41	
2.5	1.0	11	2.5	.4	-.4	1.58	
4.0	.9	8	4.5	.13	-.90	2.12	
3.0	.7	12	4.3	.23	-.63	2.07	
5.0	3.5	12	1.4	.71	-.15	1.18	
4.5	1.0	3	4.5	.65	-.18	2.12	
5.0	3.8	17	1.35	.74	-.13	1.16	
*4.0	3.5	56	1.1	.91	-.04	1.05	
*3.0	2.5	62	1.2	.83	-.08	1.1	
147.5	78.5		87.2	20.9		57.56	TOTALS

XZ PLANE SPECIMEN 2

LONG AXIS (X) (mm.)	SHORT AXIS (Z) (mm.)	(Ø)	RATIO X/Z	LOG X/Z	$(X/Z)^{\frac{1}{2}}$
5.0	3.5	8	1.43	.155	1.2
4.0	3.0	16	1.33	.124	1.15
4.5	1.25	13	3.6	.55	1.9
6.2	1.1	13	5.64	.75	2.38
3.0	.7	13	4.29	.63	2.07
3.0	2.0	7	1.5	.176	1.22
3.0	1.2	17	2.5	.4	1.58
4.0	1.5	8	2.67	.43	1.63
4.0	2.5	6	1.6	.2	1.27
5.0	3.0	10	1.67	.22	1.29
8.5	1.3	13	6.54	.82	2.56
2.5	.5	12	5.0	.69	2.24
*2.0	1.0	56	2.0	.3	1.41
3.0	2.0	22	1.5	.176	1.22
5.0	3.0	10	1.67	.22	1.29
5.0	1.2	7	4.17	.62	2.04
*1.2	1.1	62	1.09	.037	1.04
5.0	1.7	6	2.94	.47	1.71
4.0	1.8	7	2.22	.35	1.49
*1.0	.9	59	1.11	.045	1.05
2.5	.9	12	2.77	.44	1.67
4.5	.8	13	5.63	.75	2.39
4.0	.8	14	5.0	.69	2.21

LONG AXIS (X) (mm.)	SHORT AXIS (Z) (mm.)	(Ø)	RATIO X/Z	LOG X/Z	$(X/Z)^{\frac{1}{2}}$	
10.0	1.0	11	10.0	1.0	3.16	
5.0	.8	10	6.25	.795	2.5	
9.0	2.5	10	3.6	.56	1.9	
4.0	1.4	12	2.86	.46	1.7	
5.0	2.0	11	2.5	.4	1.58	
6.0	1.9	13	3.16	.49	1.78	
10.0	3.0	13	3.3	.52	1.8	
3.5	2.2	4	1.59	.20	1.26	
*3.0	2.9	62	1.03	.013	1.01	
*2.4	2.1	63	1.14	.06	1.07	
4.0	1.0	6	4.0	.6	2.0	
*7.0	.8	7	8.75	.94	2.96	
*4.2	3.8	75	1.14	.06	1.07	
2.0	1.8	45	1.11	.045	1.06	
3.0	.4	5	7.5	.88	2.79	
5.0	2.5	15	2.0	.30	1.41	
5.0	1.2	6	4.17	.62	2.04	
1.4	1.3	54	1.08	.033	1.04	
1.1	1.05	50	1.05	.02	1.02	
2.5	2.2	50	1.14	.057	1.07	
1.9	1.3	12	1.46	.164	1.21	
184.0	73.9		136.6		73.4	TOTALS